DEGREE PROJECT IN THE FIELD OF TECHNOLOGY
ENERGY AND ENVIRONMENT
AND THE MAIN FIELD OF STUDY
MECHANICAL ENGINEERING,
SECOND CYCLE, 30 CREDITS
STOCKHOLM, SWEDEN 2020

Modelling Latent Heat Thermal Energy Storage with Novel PCM Encapsulation Design

A Storage Heat Transfer and Integration Study for a Swedish Multi-Family Building Heating System

EMMA NYHOLM HUMIRE

KTH ROYAL INSTITUTE OF TECHNOLOGY
SCHOOL OF INDUSTRIAL ENGINEERING AND MANAGEMENT

KTH Industrial Engineering and Management

Master of Science Thesis

Department of Energy Technology

KTH 2020

Modelling Latent Heat Thermal Energy Storage with Novel PCM Encapsulation Design

A Storage Heat Transfer and Integration Study for a Swedish Multi-Family Building Heating System

TRITA: TRITA-ITM-EX 2020:474

Emma Nyholm Humire

Approved	Examiner	Supervisor
31st August 2020	Justin Ning-Wei Chiu	Tianhao Xu
	Industrial Supervisor	Contact person
	-	-

Acknowledgement

Firstly, I would like to thank my supervisor Tianhao Xu for providing me with this opportunity to conduct this very interesting research and for supporting and guiding me throughout this half a year of intense thesis work. Secondly, I would like to thank Justin Ning-Wei Chiu, the examiner, for always providing insightful feedback and helpful guidance. I would also like to express my gratitude to Joar Bagge for helping me in trying and challenging Matlab times.

Lastly, I want to thank my family for always supporting me. *Las quiero muchito.*

And a brief quote from a song that inspired me during this very strange year

Toda la gente me está mirando porque soy caporal
Cuando yo bailo tiembla la tierra porque soy caporal

Abstract

Thermal energy storage (TES) is the umbrella term for a number of energy storage techniques that are emerging as attractive options to even out the mismatch between production and demand of energy (e.g. electricity, heat) by storing thermal energy during valley hours and utilising the stored energy during peak hours. Latent heat thermal energy storage (LHTES) is one subcategory of TES that is interesting due to its high energy density as the process involves the phase-change of materials. New techniques for LHTES are emerging, one of them being encapsulation of the phase-change material (PCM). There are several geometries of encapsulation available on the market, such as slab-shaped and cylindrical. However, there is a research gap in investigating the heat transfer performance of more novel shapes such as quasi-ellipsoidal encapsulation. Furthermore, it is also necessary to investigate how such a LHTES system would perform when integrated with a residential heating system. To solve these two research problems, this thesis presents the findings of the transient numerical heat transfer modelling of a LHTES unit prototype with quasi-ellipsoidal encapsulation of PCMs. The thesis also investigates the techno-economic potential and potential to reduce indirect CO_2 emissions by integrating the unit with a ground-source heat pump (GSHP) for a Swedish multi-family building heating system.

Firstly, the numerical heat transfer modelling is based on a LHTES prototype developed and tested at KTH Royal Institute of Technology in Stockholm and has been performed using MATLAB® R2018b. The LHTES prototype utilises a PCM called ATP60, with a melting temperature range around 57 - 60˚C. A two-phase model as presented by Schumann in 1929 is used to model the transient heat transfer rate in the LHTES unit between the two phases: (1) the encapsulated PCMs and (2) the heat transfer fluid (HTF), which is water in this case. The MATLAB® R2018b model has been validated using experimental data for the LHTES prototype at KTH and the model shows a maximum relative error in accumulated storage capacity of 2.9%.

Secondly, the system study for the multi-family building heating system is performed in Simulink® and utilises the validated MATLAB® R2018b model of the LTHES unit. This numerical tool is specially developed for evaluating technical, economic, and environmental performance of LHTES-integrated heating systems with complex non-linear behavior in phase-change heat transfer. A fictional system in Stockholm is simulated for a week in January and the case with the LHTES is benchmarked against a baseline case with no LHTES. The benchmarking is based on parameters such as the system's electric consumption (kWh), system efficiency and electric bills. The LHTES operates according to a schedule determined from statistically established peak and valley hours of electricity prices.

The results indicate that the LHTES system allows to load-shift 27% of the electric consumption from the peak hours to valley hours, alleviating both the electricity grid and user-sides. However, this comes at the cost of increasing the total electric consumption by 7.5% in order to achieve sufficiently high temperatures from the GSHP to enable phase-change of the PCM. Furthermore, two new electricity profiles (with a greater difference between the prices at peaks and valleys) are proposed to highlight that new electricity pricing systems are needed to make the investment of storage systems like this one feasible. These findings imply high complexity in LHTES design problems for integration in heating systems, which involve not only technical assessment but also social-economic consideration for prompting LHTES to proper utilization.

Keywords: thermal energy storage, latent heat thermal energy storage, ground-source heat pump, multi-family building,

Sammanfattning

Termisk värmelagring (*eng.* TES) är en samlingsterm för ett antal energilagringstekniker som kan visa sig vara intressanta för att jämna ut skillnaden mellan produktion och efterfrågan av energi (exempelvis elektricitet, värme) genom att lagra termisk energi under timmar då efterfrågan på energi är låg (dalar) och använda den lagrade energi när efterfrågan är hög (toppar). Latent värmelagring (*eng.* LHTES) är en underkategori till TES som är intressant på grund av sin höga energidensitet i och med att processen involverar fasövergång av material. Det framträder nya tekniker för LHTES, varav en är inkapsling av fasförändringsmaterialet (*eng.* PCM). Det finns flera olika geometrier för inkapslingar tillgänliga på marknaden, exempelvis rätblocksformade och cylindriska inkapslingar. Det saknas dock forskning som undersöker värmeöverföringsprestandan hos mer ovanliga geometrier såsom kvasi-ellipsoidiska inkapslingar. Vidare är det också nödvändigt att undersöka hur ett LHTES-system skulle prestera om det integreras i ett uppvärmningssystem för bostäder. För att lösa dessa två forskningsproblem så presenteras i detta examensarbete resultatet av den numeriska modelleringen av en LHTES-prototyp (med kvasi-ellipsoidiska inkapslingar av PCM:et) och dess transienta värmeöverföringsförlopp. Vidare undersöks den tekno-ekonomiska potentialen och potentialen att minska indirekta CO_2-utsläpp genom att integrera LHTES-enheten med en bergvärmepump i ett uppvärmningssystem för ett svenskt flerfamiljshus.

Den numeriska modelleringen av värmeöverföringen utförs med hjälp av MATLAB® R2018b och baseras på en LHTES-prototyp som är utvecklad och testad vid Kungliga Tekniska högskolan (KTH) i Stockholm. LHTES-prototypen använder sig av ett PCM vid namn ATP60 som har en smältpunkt kring 57 - 60˚C. En tvåfasmodell som presenterades 1929 av Schumann används för att modellera det transienta värmeöverföringsförloppet i LHTES-enheten mellan de två faserna: (1) det inkapslade PCM:et och (2) värmeöverföringsfluiden (*eng.* HTF), som i detta fall är vatten. MATLAB® R2018b-modellen har validerats med experimentell data för LHTES-prototypen vid KTH och den uppvisar ett maximalt relativt fel i ackumulerad lagringskapacitet på 2,9%.

Systemstudien för flerfamiljshusets uppvärmningssystem utförs i Simulink® och använder sig av den validerade MATLAB® R2018b-modellen av LHTES-enheten. Detta numeriska verktyg är speciellt utvecklat för att utvärdera den tekniska, ekonomiska och klimat-prestandan hos ett värmesystem med en integrerad LHTES-enhet som uppvisar komplext, icke-linjärt beteende i fasövergångsprocessen. Ett fiktivt system i Stockholm simuleras under en vecka i januari och fallet med LHTES-enheten utvärderas och jämförs med ett referensfall utan LHTES. Utvärderingen baseras på parametrar såsom systemets elkonsumtion (kWh), systemets verkningsgrad och elkostnaderna. LHTES-enheten körs enligt ett schema som bestäms utifrån statistiskt bestämda toppar och dalar för elspotpriser.

Resultaten visar att det med LHTES-systemets hjälp är möjligt att skifta 27% av elanvändningen från topp-timmarna till dal-timmarna, vilket innebär en avlastning för både elnätet och elkonsumenterna. Detta sker dock till priset av att den totala elkonsumtionen ökar med 7,5% till följd av att höga uttemperaturer från bergvärmepumpen erfordras för att smälta PCM:et. Vidare föreslås två nya elprisprofiler där skillnaden i pris mellan toppar och dalar görs större. Dessa betonar vikten av nya elprissystem för att göra investeringar i värmelagringssystem som detta lönsamma. Studien visar på en hög grad av komplexitet då LHTES-system ska integreras med värmesystem. I designprocessen är det är nödvändigt att göra tekniska utvärderingar samt beakta sociala och ekonomiska faktorer för att se till att LHTES-enheten används på ett effektivt sätt.

Nyckelord: värmelagring, latent värmelagring, bergvärmepump, flerfamiljshus.

Preface

This master thesis presents the findings of a master thesis project carried out at the Division of Applied Thermodynamics and Refrigeration as well as the Division of Heat and Power, the Department of Energy Technology (EGI), School of Industrial Engineering and Management (ITM), KTH Royal Institute of Technology. Three papers on the main topic of latent heat thermal energy storage for application in residential heating systems constitute this master thesis, of which Paper I makes up the main body of the thesis work. The work is based on a LHTES prototype with novel PCM encapsulation design, developed as part of the EU funded H2020 project PUMPHEAT at KTH. The structure of this master thesis is as follows: firstly, Paper I presents a system analysis of integrating a LHTES unit with a residential heating system. The model of the LHTES unit used in Paper I is based on the prototype developed and tested at KTH; the LHTES prototype utilises quasi-ellipsoidal encapsulation of the PCMs. Secondly, Paper II presents the experimental and numerical characterization of the LHTES prototype; the heat transfer model developed for predicting the prototype thermal performance of was used in the system analysis as presented in Paper I. Lastly, Paper III presents the findings of numerical investigation of LHTES prototype at KTH but with cylindrical encapsulation. A brief introduction to each of the papers is given below.

Paper I, *Evaluation of latent heat storage integration in a Swedish multi-family heating system*, investigates the integration of a LHTES unit into a multi-family building radiator heating system. A fictional radiator heating system in Stockholm, Sweden was simulated for a week in January 2019 using a validated heat transfer MATLAB model for the LHTES unit.

Paper II, *Experimental and Numerical Investigation of a Latent Heat Thermal Energy Storage Unit with Ellipsoidal Macro-encapsulation*, pertains to the development and validation of the transient heat transfer MATLAB model of the LHTES prototype using quasi-ellipsoidal encapsulation. This is the model that was used in Paper I.

Paper III, *Numerical Thermal Performance Investigation of a Latent Heat Storage Prototype toward Effective Use in Residential Heating Systems*, concerns the evaluation of another storage alternative in which cylindrical encapsulation is used in the same LHTES prototype at KTH. The general idea in this paper is still on the topic of a heat pump heating system coupled with LHTES.

Publications

Paper 1: **Nyholm Humire, E.**, Xu, T., Chiu, J. N-W., 2020. *Evaluation of latent heat storage integration in a Swedish multi-family heating system* [to be submitted to *Enerstock 2021 Conference*]

Paper 2: Xu, T., **Nyholm Humire, E.**, Trevisan, S., Ignatowicz, M., Sawalha, S., Chiu, J. N-W., 2020. Experimental and Numerical Investigation of a Latent Heat Thermal Energy Storage Unit with Ellipsoidal Macro-encapsulation. [to be submitted to *Energy*]

Paper 3: Xu, T., **Nyholm Humire, E.**, Chiu, J. N-W., Sawalha, S., 2020. Numerical thermal performance investigation of a latent heat storage prototype toward effective use in residential heating systems. *Applied Energy*, 278.

Contributions of the author to the publications

Paper 1: The author was the principle contributor to the model development, simulation and result analysis as well as paper writing.

Paper 2: The author's main contribution in this paper is the development of the LHTES heat transfer modeling in MATLAB as well as validation of said model and writing corresponding sections in the article.

Paper 3: In this paper, the author's main contribution is the optimization analysis and paper writing about the capsule diameter effects on parameters like completion time and total thermal storage energy capacity of a second LHTES prototype designed for residential heating application.

Conclusions and Future Work

The main findings and conclusions of this thesis can be summarized in the following points. Firstly, in Paper III we found that reducing the diameter of cylindrical PCM capsules (from 69 mm to 15 mm) can shorten the completion time of charge/discharge by 58%/70%, whereas it also led to 23% decrease in storage capacity. This is mostly because of change in void fraction and shell volume, which should be understood well from the engineering perspective when optimizing the design. The investigation highlighted with the study on the diameter variations of the encapsulations demonstrates the process of optimization on a component level for heating application. Secondly, in paper II, it is possible to accurately model the transient heat transfer process of the LHTES unit using a two-phase packed bed model for a novel LHTES design using ellipsoidal encapsulation of PCM. The accuracy is found to be 2.9% as compared with experimental data, with use of an extended lumped capacitance method shape approximation to simplify the phase-change heat transfer process. This simplified model permits fast and accurate prediction of heat transfer for this novel design, which validates its convenient use in energy system modelling where the integration of novel storage design is simulated. Thirdly, the performance of the LHTES unit modelled in Paper II is evaluated when integrated to a heating system. The 7.5% increased electricity consumption with the integration indicates that the LHTES-integration is a complex design problem which is highly dependent on (1) system layout design, (2) control strategy and (3) choice of PCM. Nevertheless, the cost-effective use (considering a simple payback time 5 years) of it is prospected with a proposed future scenario with subsidy and negative valley electricity prices to encourage demand-side load shifting. Comprising of work shown in the three appended papers, this thesis investigates LHTES for heating application from heat transfer modelling and optimization from the component level, and LHTES unit integration and control strategy for operation from the system level. This holistic research approach promotes understanding of the effects and design aspects of integrating LHTES units into heating systems and provides recommendation for grounding LHTES application on the user's perspective.

Regarding future work it is necessary to:

- investigate if discretizing the encapsulation (and not use an extended lumped capacitance method) could increase the accuracy of the temperature evolution results output from the MATLAB model
- validate the MATLAB model for other encapsulation geometries
- investigate other system layout design options for the LHTES-integrated system, where for example the LHTES unit could be connected to the desuperheater of the GSHP
- investigate if other control strategies could increase the performance of the LHTES-integrated system
- investigate other types of PCMs with lower melting points to see if there is a PCM better suited for the particular heating system

Table of Contents

Abstract……... 1
Sammanfattning…….. 2
Preface…… 3
Conclusions and Future Work…… 5
Paper I……. 7
Paper II……... 15
Paper III…….. 16
Appendix…… 45

Paper I

Evaluation of latent heat storage integration in a Swedish multi-family heating system

Emma Nyholm Humire, Tianhao Xu, Justin Ning-Wei Chiu
Department of Energy Technology, KTH Royal Institute of Technology, 100 44, Stockholm, Sweden

ABSTRACT

Thermal energy storage (TES) is a feasible demand side management tool for implementing peak load shifting to increase system efficiency and to reduce system costs. As a result, indirect carbon dioxide (CO_2) emissions and electricity grid stress related to peak plant operation can potentially be mitigated. In this study, a quasi-steady state model is built with MATLAB® R2018b and Simulink® to investigate the technical, economic and environmental potential of integrating a LHTES unit into a Swedish multi-family radiator heating system consisting of a ground-source heat pump (GSHP) and electric heaters. The studied LHTES utilizes a novel PCM encapsulation design and is integrated to GSHP on the condenser side for charging during valley hours and to the radiators for covering peak heating demand during discharging according to a developed control strategy. The LHTES integrated system is benchmarked against a baseline system on operational performance indicators like total electric consumption and electricity costs for a week in January 2019.

The results indicate that it is possible to shift 27% of the peak electricity consumption using the LHTES. The electricity costs increased by 6.3% due to a 7.5 % increase in electrical consumption to the GSHP necessary to raise the condensation temperature to enable melting of the PCM. To investigate possible future scenarios where profitable LHTES installation can be granted, two new hourly-based electricity price profiles are proposed, and with the first profile the system operational costs can break-even as compared to the baseline case and with the second profile the operational costs can be reduced, achieving a simple payback period of 5 years. This study highlights the need for new electricity pricing systems to make storage investments economically feasible as well as the complexities of integrating LHTES into heating systems.

Keywords: Latent heat thermal energy storage, ground-source heat pump, residential heating, multi-family building.

NOMENCLATURE

Abbreviations

A_{temp}	floor area of space heated above 10˚C, defined by The Swedish National Board of Housing [m^2]
U-value	heat transfer coefficient [W/K]
SoC	State of Charge [%]
COP_1	Coefficient of Performance of heating
DOT	Dimensioning Outdoor Temperature
IN	Indoor
cond,in	Condenser inlet
cond,out	Condenser outlet
ASHP	Air-source heat pump
GSHP	Ground-source heat pump
HTF	Heat transfer fluid
LHTES	Latent heat thermal energy storage
PCM	Phase-change material
SDG	Sustainable Development Goal
SPP	Simple Payback Period
WPF	Weekly Performance Factor
TES	Thermal Energy Storage
VAT	Value Added Tax

1. INTRODUCTION

The Sustainable Development Goals (SDGs) are helpful in indicating the most fruitful directions for sustainable development of energy utilisation. SDG 7 Affordable and Clean Energy calls for an increase in energy efficiency as well as access to reliable energy by year 2030. (United Nations, 2015) In Sweden, the energy consumption of the residential and service sector corresponds to 40% of Sweden's total energy consumption, of which the residential households represent 59% of the total amount (Energimyndigheten, 2020). Since this is a large sector, a slight increase in the energy efficiency of this sector would contribute significantly to the overall energy balance. Another important aspect of sustainability is the indirect carbon dioxide (CO_2) emissions related to power consumption in households. The mass of CO_2 emitted per unit of electricity production varies hourly over a day (IEA, 2020), due to fossil fuels with high CO_2 emission being used for power generation during peak hours (Hirmiz, et al., 2019). One

possible way to decrease CO_2 emissions is to utilise energy storage, especially thermal energy storage (TES) to shift the power and heat demand by storing heat during valley hours and later using it during peak hours. If electricity is used to produce heat (e.g. via a heat pump) this could also result in an economic gain since electricity prices vary throughout the day with power demand. Furthermore, since the load on the electricity grid in Sweden is increasing with a growing population particularly in urban areas (IVA, 2017), load shifting with storage offers a possibility to alleviate the load on the electricity grid during peak hours.

Latent heat thermal energy storage (LHTES) is one type of TES. One type of configuration for LHTES is encapsulation (Cabeza & Oró, 2016) There are different ways of integrating a storage to a heating system, one is coupling with heat pumps (HPs). Ground source heat pumps (GSHPs) constitute half of heat pump installations in multi-family dwellings in Sweden (Energimyndigheten, 2016), mainly for their stable heating capacity throughout heating season due to low variations in heat source temperature (SGU, 2016)

In 2014, Fischer et al. investigated the coupling of a sensible TES with an air-source heat pump (ASHP) for a multi-family dwelling in Germany and found that utilising storage could help in decreasing system costs (Fischer et al., 2014). Hirmiz et al. studied the integration of a hybrid sensible and LHTES system with GSHP for a single-family house in the UK, utilising slab-shaped encapsulation of the PCMs. One of their conclusions was that the high temperatures required to melt the PCMs caused the COP to drop thus decreasing overall system efficiency while also increasing system costs as a result of increased power demand to the GSHP (Hirmiz, et al., 2019).

No study has yet been done analysing HP heating system behaviour and performance when coupled with LHTES in a radiator heating system for a multi-family dwelling. In this article, the transient storage performance of a LHTES unit with novel PCM macro-encapsulation shaped ellipsoids is modelled. This storage model has been validated through comparison to prototype testing obtained at KTH Energy Technology Department (European Union, 2020). The hourly energy use and electricity cost in such a system during a heating-season week is simulated for the LHTES-integrated heating system and benchmarked against a baseline system without load shifting. Furthermore, new electricity price profiles are proposed to incentivize LHTES installation.

2. METHODOLOGY

2.1 Building Heating System and Mathematical model

A fictional building heating system representing a typical Swedish multi-family building, with construction year 1986-1995, has been modelled. Firstly, the heat demand of the building was calculated with the input parameters, as provided in table 1, a dimensioning outdoor temperature (T_{DOT7}) of -13.7˚C and a desired indoor temperature (T_{IN}) of 20˚C. The heat demand at T_{DOT7} was 40.2 kW. T_{DOT7} is taken at the building's time constant of 6.4 days, according to Boverket's method (Boverket, 2012). Hourly outdoor temperature data from 2019 for the Stockholm-Bromma area was collected from (Sveby, 2019), the industry standard for building related energy calculations.

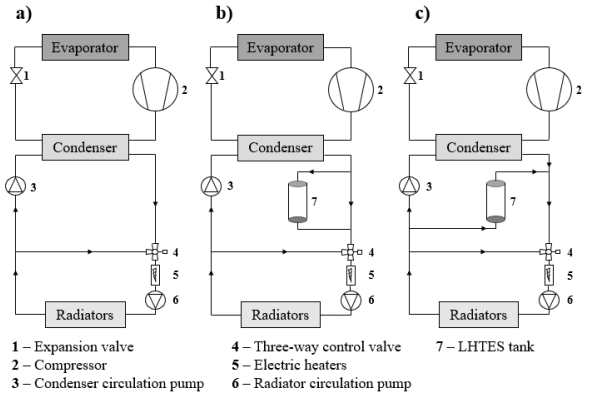

Fig. 1 The building heating system for a) the baseline case and b) and c) both illustrate the case with LHTES integrated. In Fig. 1 b) the charging mode is illustrated and in Fig. 1 c) the discharging mode.

Table 1 Input data for the multi-family residential building.

Property / Surface	Walls	Roof	Windows	Floor area[a]
Area [m²]	560	470	180	1400
U-value [W/m²·K]	0.22	0.15	1.8	-

[a]The total floor area of the building

The baseline heating system (seen in Fig.1 a) of the building consisted of a GSHP (utilising propane as the refrigerant) and electric heaters that provide heat to radiators in the multi-family building's apartments. A radiator model with 455 W output heat at radiator supply and return temperatures of 55˚C/45˚C (Purmo, 2017) was chosen for the building's heating system. The GSHP in the system model was based on a GSHP in the NxtHPG project (European Commission, 2019), but modified to have a variable speed compressor instead of an ON/OFF control only. The pumping power for the borehole field was neglected due to complexities in the borehole heat exchanger design and left for future work. The GSHP was modelled by creating a polynomial for the Coefficient of Performance of heating (COP_1) as a function of the inlet and outlet temperature of the secondary fluid in the condenser (secondary fluid temperature on the heat source side was assumed constant throughout the investigated week). To generate this polynomial, the vapor-compression unit modelling software IMST-ART (IMST-ART, 2019) was used to model the GSHP. Firstly, an already validated IMST-ART model of the GSHP showing less than 2.8% difference in COP_1 as compared with experimental data (Piscopiello, et al., 2016) was modified to have a variable speed compressor. Secondly, a parametric sweep of a total of 84 cases with different inlet and outlet temperatures of the secondary fluids was performed to generate a COP_1

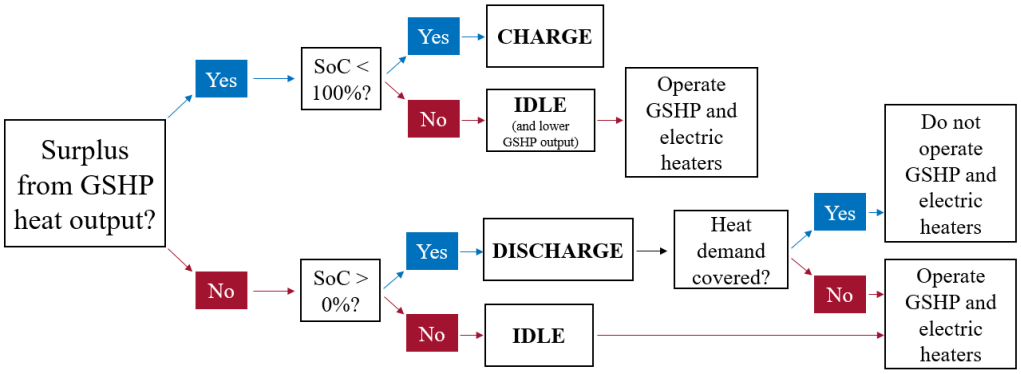

Fig 3. The control strategy of the system with LHTES integrated

performance map. The conditions for the parametric sweep were chosen to cover the different possible temperature cases in the system, with the lowest outlet temperature of 25 ˚C and the highest outlet temperature of 65˚C. The highest outlet temperature of 65˚C was used to ensure phase-change of the PCMs, as presented in the section 2.2.

2.2 LHTES model

A macro-encapsulated LHTES unit with commercial quasi-ellipsoid capsules (Fig. 2) was modelled based on Schumman's model (Schumann, 1929). The encapsulations are filled with a PCM named ATP60, which has a melting and solidification point in the temperature range of 57-60˚C (Axiotherm, 2018). The LHTES model is a one-dimensional, transient heat transfer model of an existing LHTES prototype utilising encapsulation, as illustrated in Fig. 2. This heat transfer model has been validated by experimental results, showing a maximum relative error of 2.9% for the accumulated storage capacity.

The LHTES model was scaled up with the same storage density as the prototype and was dimensioned to cover the heating demand during the three consecutive hours in the morning when the heat demand peaks, namely in January, February, March, November and December. The storage dimensions for the LHTES tank used in the system model are shown in Table 2.

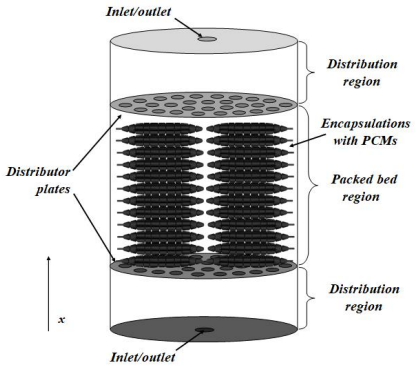

Fig. 2 The LHTES tank with distribution regions and packed bed region (with encapsulated PCMs). Axis "x" indicates the direction of the flow of the HTF through the tank and is the one dimension considered in the heat transfer model.

Table 2 Storage tank dimensions

Storage density [kWh/m³]	Volume [L]	Maximum storage capacity [kWh]
35.96	1532	68.98

2.3 Simulink model, LHTES integration and control strategies

A system model of the multifamily building's space heating system was created using Simulink®, a modelling tool in MATLAB® R2018b environment. This system was simulated for an entire week in January of 2019 with a time step of 1 hour.

The control strategy of the system consists of mainly three modes for the LHTES: (1) Charge, (2) Discharge and (3) Idle. In the charge mode, the outlet temperature of the secondary fluid in the condenser was manually raised to 65˚C and a surplus of heating output from the GSHP could be stored in the LHTES. At the same time, the heating demand of the building is met by the GSHP and electric heaters. In the discharge mode, the heating demand was to be met primarily by the LHTES, secondly the GSHP and lastly the electric heaters, here the LTHES was discharged with the return water from the radiators. In the idle mode, the LHTES stood by and the heat loss coefficient was obtained experimentally.

A bin hour analysis of the hourly electricity prices was performed to determine the charge, discharge and idle hours. Peak hours correspond to the three hours with highest electricity price and valley hours correspond to the 8 hours with the lowest electricity price. One operational scheme from the statistical analysis is to discharge LHTES between 8-10 AM and charge it between 4-7 AM. The charge hours were shortened from 8 to 4 hours based on the simulations indicating that the charge process requires less than 8 hours for full or near-full charge (SoC 100%).

A flow chart summarizing the control strategy for the system operations is illustrated in Fig. 3. In the first step, as shown as the leftmost box in the flow chart, the surplus in the heating capacity of the GSHP to the current heat demand is checked when outlet temperature of the condenser is manually raised to 65˚C. However, if the SoC was already 100% during the designated charging hours, the temperature would be lowered from 65˚C to the radiator supply temperature and the

system would operate as in the baseline mode (i.e. "Idle" mode). Furthermore, the scheme of defined valley and peak hours created from the bin hour analysis were also applied to the control scheme. For example, the charge mode was only an option during the scheme's defined valley hours and discharge mode during the defined peak hours.

2.4 Methodology of evaluation on storage integration effect

To evaluate the effect of the integration of LHTES in the radiator heating system, five main indicators were calculated: (1) the system's total electrical consumption [kWh], (2) the GSHP's Weekly Performance Factor (WPF_1), (3) the electric costs and (4) indirect carbon dioxide emissions related to power consumption and (5) percentage shifted energy. The first two give an indication of the technical potential, while the third and the fourth give an indication on economic and environmental potential, respectively.

The WPF_1 of the entire system was calculated for the simulated period of 1 week, according to eq. (1). The WPF_1 is defined as the ratio of the sum of output from the GSHP to the total electric power required by the GSHP, circulation pumps and the electric heaters in the system during the simulated week.

$$WPF_{system} = \frac{\sum_{t=0}^{T} Q_{GSHP}}{\sum_{t=0}^{T} E_{GSHP} + E_{pumps} + E_{electric\ heaters}} \quad (1)$$

Data on hourly market electricity prices were retrieved from Nordpool (2020), while quotes for energy taxes on electricity and electricity network tariffs were retrieved from the electricity distribution company Ellevio (2020b), (2018). Ellevio's network tariffs consist of both a fixed monthly fee as well as a variable fee per MWh of electricity used. The values are summarized in Table 3. Furthermore, in order to evaluate how storage investments could be encouraged, we proposed two new electricity price profiles which are beneficial for both the network and the user. In these two proposals the electricity price during peaks and valleys are amplified; the first profile aims to find a break-even point in operational costs while the second aims to achieve a Simple Payback Period (SPP) of 5 years. In the second profile the electricity valley price is set negative as seen in countries like Germany, for example, where the electricity price has historically dropped as low as -150€/MWh and peaked at 500€/MWh (Fanone, et al., 2011).

Table 3 Input data for energy taxes and network tariffs. The energy tax includes value added tax (VAT).

Energy tax [SEK/MWh]	Network tariffs	
	Fixed [SEK/month]	Variable [SEK/MWh]
433.8	1310	275.0

The indirect CO_2 emissions from the electric power consumption of circulation pumps and the heat pump compressor during the simulated period was estimated using data of hourly CO_2 emissions per produced kilowatthour of electricity. The data represents an average for the European Union (IEA, 2020). During off-peak hours, the emissions are on average around 65 kg CO_2/MWh less than during peak hours. The amount of shifted electricity consumption in the load shifted scenario and the total during peak hours (8-10 AM) in the baseline case are compared, the ratio between the two (0%-100%) indicates the extent of peak load shifting with the investigated control scheme and LHTES installation. Lastly, the SPP is calculated according to eq. (2). When calculating the investment costs, it is assumed that a subsidy of 50% can be acquired for the PCM encapsulation costs and that the investment costs for the storage tank would lower per cubic meter of tank volume as the tank size increased (Hedegaard, et. al, 2012). The values used for the investment costs are summarized in Table 4.

$$SPP = \frac{\text{Investment costs}}{\text{Annual savings}} \quad (2)$$

Table 4 Input data for investment costs of PCMs (including encapsulation) and storage tank.

PCM [€/piece][a]	PCM [€/piece][b]	Storage tank [€/100 L]	Total investment costs [€]
5.2	2.6	121	5491

[a]Unsubsidized , [b]Subsidized 50%

3. RESULTS AND DISCUSSION

The results for the comparison between the baseline case and the load-shifted case (with the LTHES integrated in the building's heating system) are presented in Table 5. Firstly, the total electric consumption increased by 7.5% in the case with the LTHES. This increase in electric consumption is caused by the increased compressor power necessary to raise the outlet temperature of the secondary fluid (by raising the condensation temperature) in the condenser to 65˚C during charge mode. This in turn causes the COP_1 of the GSHP to drop during the charge hours, as shown in Fig. 4 and thus the WPF_1 for the simulated period decreases. The average decrease of COP_1 for the simulated period is 17%. The decrease in WPF_1 from the baseline case to the LTHES integrated case corresponds to 3%.

Table 5. A summary of the results for the simulated 1st week of January 2019 for the baseline case and the load shifted case, including electricity bills for the proposed electricity price profiles.

	Baseline case	Load shifted case
Total electrical consumption [kWh]	*2280*	*2452*
WPF_1 [-]	*1.59*	*1.54*
Shifted energy [%]	-	*27*
Indirect CO_2 emissions [kg]	*543*	*576*
Electricity bill [SEK][a]	*3034*	*3226*
Electricity bill [SEK] with "break-even" profile	*2881*	*2881*
Electricity bill [SEK] with "lower costs" profile	*2742*	*2529*

[a] 1 SEK = 10.33 €

Although the total electric consumption as well as WPF_1 decreased when integrating the storage, it was possible to

shift the electric load by 27% during the peak hours, leading to a lower peak load on the electricity grid.

With the issue of the increased temperature in mind, it is worthwhile investigating the same system using a PCM with lower melting/crystallisation point. Avoiding high outlet temperatures from the condenser due to lower melting points could be beneficial from the heat pump operating perspective. However, issues could instead arise if a very low storage inlet temperature (i.e. radiator return temperature) is needed for the discharge mode to ensure solidification of the PCM, as such a radiator heating system with lowered operating temperatures might not suffice thermal comfort requirement in Nordic climates. If the baseline heating system is to be adapted for LHTES integration with a low phase-transition point, it could be necessary to lower the temperature of the returning water from the radiator by means of a heat exchanger or coolers, which would further increase the capital expenditure of the storage system.

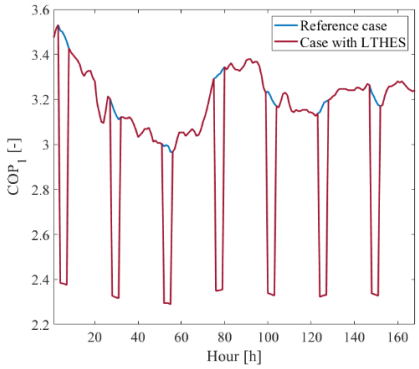

Fig. 4 The hourly variation of COP_1 for the baseline case compared to the case with LHTES for the simulated period.

Secondly, the indirect CO_2 emissions related to the electric power consumption of the system increased by 5.7%. This is most likely caused by (1) the overall increase in total electric consumption and (2) the scheme for the LHTES aimed to shift load from the morning hours based on the bin hour analysis. However, the CO_2 emissions from electricity production are the highest during the afternoon according to the data from the European Union. Thus, future studies on this system could investigate a scheme that aims to load
shift the afternoon hours.

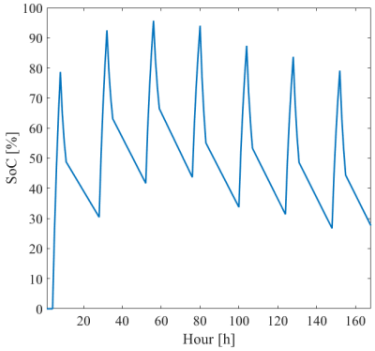

Fig. 5 The hourly variations of the LHTES State of Charge (SoC) for the simulated period.

The variation of the SoC of the LHTES during the simulated period is shown in Fig. 5. The figure shows a cyclic behaviour of continuous charge and discharge during the week. However, it is observed that the storage does not discharge completely at any point during the week, but instead discharging down to around 30-50% SoC. There are a number of possible explanations for this; the LHTES runs on a control strategy that is governed by several different parameters such as defined peak and valley hours, GSHP available heat output at the current hour and SoC of the LTHES. It is possible that the defined peak hours used for discharging the storage did not provide enough time to completely discharge. However, the time for discharging and charging is related to the flow rate of HTF supplied to the storage. Thus, this also brings up the necessity of further investigating into optimization of flow rates in the system.

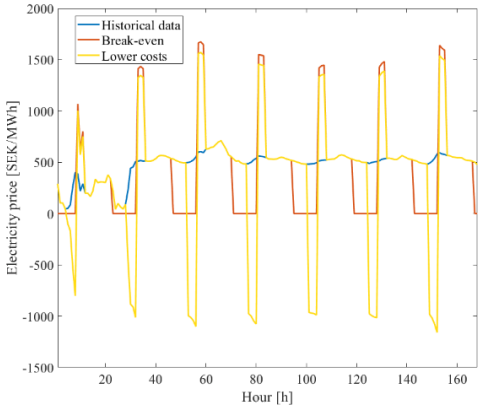

Fig. 6 The historical electricity prices from Nordpool (blue) and the two proposed electricity price profiles; break-even (orange) and lower operational costs (yellow).

Despite the benefit of peak load shifting by 27%, the total electricity costs of the system increased by 6.3% from the baseline. Nonetheless, with the two proposed electricity price profiles illustrated in Fig. 6 it is possible to achieve (1) break-even and (2) SPP of 5 years. The electricity costs for the "*Lower costs"* electricity price profile are presented at the bottom of Table 5. Both electricity profiles have a greater difference between peak and valley hour prices than the historical electricity price data from Nordpool, the electricity trade platform in Nordic countries. The "*Break-even"* electricity profile sets the electricity price to 0 SEK/MWh during valley hours and has higher prices during peak hours compared to the "*Lower costs"* profile, which has negative prices during valley hours but slightly lower peak prices than "*Break-even"*. This tariffing system is possible if the storage is operated by the grid and utility companies where they see grid alleviation and marginal fossil fuel based energy generation are with high priority. The saving in electricity bill was calculated as 213 SEK for the evaluated week, corresponding to 2790 SEK per MWh of shifted peak electricity demand in the "*Lower costs"* case. The annual saving was estimated as 11 kSEK, assuming similar peak load shifting was extended to all weeks in a year. These results highlight the importance of designing electricity pricing systems with negative on-peak electricity tariff, which has been practiced in Germany (Fanone, et al., 2011) to make storage systems, like this one, feasible investments with necessary subsidization.

Finally, the results raise awareness of the complexity of integrating LHTES into heating systems. The choice of PCM with the most suitable phase change temperature has a great impact on the efficiency of the system as it imposes limitations on the temperature conditions for the heating system (in this case the heat pump) to ensure phase change in the LHTES. In this study, only one system configuration was investigated but further work will be done in finding the optimal system configurations. One option is to couple the LHTES to the desuperheater of the GSHP, which is beneficial for a PCM that requires slightly higher temperatures for phase-change. Furthermore, further studies should be performed on optimizing the control strategy and operational schemes of the LHTES. A machine learning oriented control strategy considering real-time electricity prices and model predictive control accounting for valley/peak hours and user behaviours can be used.

4. CONCLUSIONS

In this work, the techno-economic-environmental potentials of integrating a LTHES in a multi-family dwelling's heating system in Stockholm, Sweden with a GSHP have been investigated for a week in January using a system model in Simulink. The following conclusions can be made from the study:

(1) Using the particular LHTES and the fixed control strategy enables 27% of the peak electric consumption to be shifted to valley hours. It however raises the total electric consumption by 7.5% and leads to a 3% decrease in WPF_1 due to the mandatory increase in condensation temperature of the GSHP to melt the PCM during charge mode. CO_2 emission also increases by 5.7%

(2) Integration of TES into a heating system does not guarantee increased efficiency and thus it is necessary to optimize system layout as well as the control strategies. One optimization point is to choose a PCM with a lower melting point to avoid raising the condensation temperature in the GSHP during charge mode. This however lowers the discharge temperature.

(3) With a proposed electricity price profile with negative electricity tariff during valley hours, the electricity bill for the particular week can be reduced, corresponding to a normalized weekly saving of 2786 SEK/MWh shifted peak electricity demand. A simple payback period of 5 years can be achieved with this profile as well as subsidies for the encapsulation investment. With this newly proposed electricity price system the storage investment can be encouraged. It has the potential to reduce stress on the utility side, the electricity network and the user-side as well as to aid in reaching the sustainability goals of reliable energy supply.

Future studies include investigation of PCMs with lower melting points to avoid high outlet temperatures from the condenser and evaluation of the saving potentials with an alternative discharge/charge scheme that load shifts during high emission marginal fossil fuel based peak hours. Finally, optimizations in system design (e.g. connecting the LHTES to the desuperheater during charge mode instead of condenser of the GSHP) and flow rates control are necessary to be fully investigated for maximizing the techno, economic, and environmental benefits of such a system.

ACKNOWLEDGEMENT

PUMPHEAT project (funded by EU Horizon 2020, grant number 764706) are acknowledged for the financial supports.

5. REFERENCES

Axiotherm, 2018. *Data sheet ATP 60*. [Online] Available at: https://www.axiotherm.de/en/download/project/productdatasheet/file/20/ [Accessed 2020 07 03].

Boverket, 2012. *Handbok för energihushållning enligt Boverkets byggregler – utgåva två*, pp.35-37.

Cabeza, L. F., Oró, E., 2016, *7 – Thermal energy storage for renewable heating and cooling systems*. [e-book] Woodhead Publishing Available at: ScienceDirect https://www-sciencedirect-com.focus.lib.kth.se/science/article/pii/B978178242213600007 2 [Accessed 2019 12 14], pp. 142-145, 147.

Ellevio, 2020a. *Våra elnätspriser*. [Online] Available at: https://www.ellevio.se/privat/elnatspriser-och-avtal/se-vara-priser/ [Accessed 2020 06 14].

Ellevio, 2020b. *Energiskatt på el*. [Online] Available at: https://www.ellevio.se/privat/elnatspriser-och-avtal/energiskatt/ [Accessed 2020 06 14].

Ellevio, 2018. *Elnätspriser för Stockholm från och med 1 oktober 2018*. [Online] Available at: https://www.ellevio.se/globalassets/uploads/dokument/prislistor-2019/prislistor-privat-2019/sakr_sth_181001_v19.pdf [Accessed 2020 06 14].

Energimyndigheten, 2016. Energistatistik för flerbostadshus 2016. *Energy statistics for multi-dwelling buildings in 2016*. [Online] Available at: https://www.energimyndigheten.se/globalassets/statistik/bostader/energistatistik-for-flerbostadshus-2016.pdf [Accessed 2020 07 08], p.20.

Energimyndigheten, 2020. *Energiläget 2020*. [Online] Available at: https://energimyndigheten.a-w2m.se/Home.mvc?ResourceId=168344 [Accessed 2020 06 18]. p.55

European Commission, 2019. *Next Generation Heat Pumps working with Natural Fluids*. [Online] Available at: https://cordis.europa.eu/project/id/307169 [Accessed 2020 07 10].

European Union, 2020. *PUMPHEAT*. [Online] Available at: https://www.pumpheat.eu/ [Accessed 2020 08 21].

Fanone, E., Gamba., A., Prokopczuk, M., 2011. The case of negative day-ahead electricity prices. *Energy Economics*, 35, p.23

Fischer, D. Rivera Toral, T. Linberg, K. B., Wille-Haussmann, B., Madani, H. 2014. Investigation of Thermal Storage Operation Strategies with Heat Pumps in German Multi Family Houses. *Energy Procedia,* 58.

Hedegaard, K., Vad Mathiesen, B., Lund, H., Heiselberg, P., 2012. Wind power integration using individual heat pumps – Analysis of different storage options. *Energy*, 47 (1), pp.284-293.
Hirmiz, R., Teamah, H. M., Lightstone, M.F., Cotton, J. S., 2019. Performance of heat pump integrated phase change material thermal storage for electric load shifting in building demand side management. *Energy and Buildings*, 190.
IEA, 2020. *Average CO2 emissions intensity of hourly electricity supply in the European Union, 2018 and 2040 by scenario and average electricity demand in 2018*. [Online] Available at: https://www.iea.org/data-and-statistics/charts/average-co2-emissions-intensity-of-hourly-electricity-supply-in-the-european-union-2018-and-2040-by-scenario-and-average-electricity-demand-in-2018 (Updated 15th January 2020) [Accessed 2020 07 07].
IMST-ART, 2019. *IMST-ART Advanced Refrigeration Technologies*. [Online] Available at: http://www.imst-art.com/ [Accessed 2020 07 10].
IVA, 2017. *Reliability in Sweden's electricity system A project report IVA Electricity Crossroads project*, p.6
Nordpool, 2020. *Historical Market Data*. [Online] Available at: https://www.nordpoolgroup.com/historical-market-data/ [Accessed 2020 06 14].
Piscopiello, S., Mazzotti, W., Nota, C., Sawalha, S., 2016. Perfomance evaluation of a large capacity water-water heat pump using propan as refrigerant. 12th IIR Gustav Lorentzen Natural Working Fluids Conference. Edinburgh, United Kingdom, 21-24 August 2016.
Purmo, 2017. *TEKNISK BROSCHYR PANELRADIATORER 7/2017*. [Online] Available at: https://www.purmo.com/publisher/online-view.php?doc=/docs/PURMO_Teknisk_broschyr_panel_0717_SE_web.pdf&locale=sv-SE#page=30 [Accessed 2020 07 01].
Schumann, 1929. HEAT TRANSFER: A LIQUID FLOWING THROUGH A POROUS PRISM. *, Journal of the Franklin Institute,* 208 (3) (1929) 405–416.
SGU, 2016. *Geologisk information för geoenergianläggningar – en översikt*. [Online] Available at: http://resource.sgu.se/produkter/sgurapp/s1616-rapport.pdf [Accessed 2020 07 08], p.5.
Sveby, 2019. *Sveby Branschstandard för energi i byggnader*. [Online] Available at: http://www.sveby.org/ [Accessed 2020 06 14].
Sveby, 2012. *Brukarindata bostäder*. [Online] Available at: http://www.sveby.org/wp-content/uploads/2012/10/Sveby_Brukarindata_bostader_version_1.0.pdf [Accessed 2020 06 14].
United Nations, 2015. *7 Affordable Energy*. [Online] Available at: https://www.un.org/sustainabledevelopment/energy/ [Accessed 2019 12 13].

Paper II **(under journal submission and removed from current public version)**

Paper III

Numerical Thermal Performance Investigation of a Latent Heat Storage Prototype toward Effective Use in Residential Heating Systems

Tianhao Xu*, Emma Nyholm Humire, Justin Ning-Wei Chiu, Samer Sawalha

Department of Energy Technology, KTH Royal Institute of Technology, 100 44 Stockholm, Sweden.

Abstract

Latent heat thermal energy storage has been receiving increasing interests in residential heating applications. In this paper, a numerical heat transfer model was built with finite element method for a cylindrically encapsulated latent heat storage prototype and used for investigating its thermal performance optimization measures. The model was validated against four sets of experimental results for both charge and discharge, as the difference in accumulated storage capacity between simulation and experiment is less than 4%. Transient storage inlet boundary conditions were set in simulation for discharge considering the thermal output from the coupled radiators. The results of the optimization analyses show that: 1) reducing the diameter from 69 mm to 15 mm shortens the completion time of charge and discharge by up to 70%, however, at the expense of 23% decrease in total storage capacity; 2) using parabolic or linear time-increasing heat transfer fluid flowrate profiles than a time-constant one extends around twofold the useful discharge timespan; 3) increasing the storage vessel diameter from 0.6 m to 0.7 m and to 0.8 m prolongs the useful discharge timespan from 2 hrs to the recommended 3 hrs, though the further enlargement to 0.8 m results in a lower state of charge after 3 hrs due to increase in unexploited storage capacity. From the numerical optimization study, we proposed a storage design adjustment of using 15 mm-diameter phase change material capsules in a 0.7 m-diameter cylindrical storage vessel, coupled with a parabolic flow strategy, to improve the storage on-peak discharging performance.

Keywords: Phase change material; heat transfer simulation; thermal performance investigation; residential heating system; cylindrical encapsulation.

*Corresponding authors. Tel.:+46 720325022; E-mail addresses: txu@kth.se

Nomenclature

$\vec{u}$	HTF flow velocity field [m/s]
a	radiator exponential [-]
A_{cs}	cross-sectional area of storage tank [m^2], 0.283 m^2 in the prototype design
$c_{p,eff}$	effective specific heat of PCM [kJ/(kg·K)]
$c_{p,f}$	specific heat of HTF (water) [kJ/(kg·K)]
D_{cap}	PCM capsule cap diameter [mm]
D_h	Hydraulic diameter of HTF channel [m]
D_i	PCM capsule inner diameter [mm]
D_o	PCM capsule outer diameter [mm]
D_{tank}	Storage tank inner diameter [m], 0.6 m in the prototype design
k	thermal conductivity [W/(m·K)]
n	Loadable number of capsules in storage [-]
N_t	time step in LHTES heat transfer simulation [-]
P_{rad}	radiator heating power [kW]
P_{tes}	LHTES charging/discharging thermal power [kW]
Q	thermal energy storage capacity (accumulated or total) [kWh]
q_h	convective heat source term between HTF and PCM [W/ m^3]
SoC	state of charge [%]
T	temperature [^{o}C]
t	time [s]/[hr]
T_0	storage initial temperature before charge/discharge [^{o}C]
T_{fd}	radiator forward temperature [^{o}C]
T_{in}	HTF storage inlet temperature [^{o}C]
T_{out}	HTF storage outlet temperature [^{o}C]
T_{PCM}	experimental average PCM temperature in storage [^{o}C]
T_r	radiator return temperature [^{o}C]

T_{room}	indoor thermal comfort temperature [°C]
UA	UA-value [kW/K]
u_f	Average HTF flow velocity in the central chamber [m/s]
u_z	HTF flow velocity in the gravitational direction at the storage inlet [m/s]
V_{by}	HTF flowrate in by-pass line [m^3/h]
V_f	HTF flowrate in storage [m^3/h]
V_{rad}	HTF flowrate in the hydronic radiator system [m^3/h]
V_{tank}	inner volume of the storage vessel [m^3], 0.382 m^3 in the prototype design

Greek symbols

ρ	density [kg/m^3]
μ	dynamic viscosity [Pa·s]
ε	void fraction [-]

Subscripts

eff	PCM effective
exp	experiment
f	HTF
in	storage inlet
out	storage outlet
p	PCM
rad	radiator
s	solid
sim	simulation
comp	completion status

Abbreviations

BDF	backward differentiation formula
DHW	domestic hot water
FEM	finite element method
HTF	heat transfer fluid
LHTES	latent heat thermal energy storage
LMTD	log mean temperature difference
PCM	phase change material
Re	Reynolds number
TES	thermal energy storage
T-history	temperature-history

1. Introduction

Proper integration of thermal energy storage (TES) can bring positive flexibility to energy system management including residential heating. Effective storage design procedure with use of latent heat thermal energy storage (LHTES) is however lacking in the literature. Here, experimentally verified storage model for LHTES design optimization and ideal operational strategies determination are conducted.

In a typical heat load shifting application, an ideal strategy is to fully charge the TES with surplus solar heat or heat produced with off-peak electricity and then to release such stored heat to fulfil heating demands during unavailable or unfavourable heat generation periods [1]. Heat can be stored in different forms; LHTES normally features higher complexity than sensible due to the use of phase change material (PCM) [2]. This complexity has been addressed in literature mainly from three aspects toward successful application of LHTES in energy systems: PCM phase equilibrium assessment (e.g. [3]), heat transfer analysis (e.g. [4]), and storage operational strategy investigation (e.g. [5]).

A number of previous research work aimed at improving heat transfer aspects in LHTES components and at accurately predicting LHTES non-linear thermal behavior for promoting understanding on performance control. For residential heating applications, Regin, Solanki, and Saini [6] compared performance of spherically encapsulated paraffins (peak melting temperature at 59.9°C) at different capsule radii, and revealed that reducing the radius from 60 mm to 20 mm shortens the completion time of melting by 24%. Gracia, Oró, Farid, and Cabeza [7] tested 40 mm-diameter cylindrical encapsulation in a 0.18 m^3 tank and validated a numerical heat transfer model, with which the storage performance at different capsule diameters ranging from 16 mm to 80 mm was simulated; the results showed that, as compared to 80 mm, a capsule diameter of 16 mm shortens melting process by 52% but decreases heat storage capacity by 20%. These studies imply that accelerating charge and discharge has been one of the major objectives in latent heat storage heat transfer analysis. Prieto, Suárez, and González [8] developed a numerical model for simulating the thermal performance of a rectangular latent heat storage unit using RT60 as the main heat storage material for household heating systems. In this work, numerical parametric studies on PCM thickness and heat exchanger orientation are performed, suggesting that using 30 mm-thick PCM plate in a horizontally placed storage unit leads to highest heat transfer rate. Wang, Yu, and Ling [9] performed both experimental and numerical investigations to evaluate heat transfer improving measures in a sodium acetate trihydrate based latent heat storage system, which is suitable for heating applications. The results in this work indicate that, adding metal fins to the storage chamber can shorten charging/discharging time by up to 27% due to heat transfer surface area extension.

In storage operation, on the other hand, Agyenim and Hewitt [10] tested a finned LHTES heat exchanger with RT58 and, considering electricity tariff profiles in the UK, specified the testing timespan at 4 hrs and 7 hrs for LHTES to discharge heat to radiators. They concluded that increasing PCM temperature from 62.9°C to 76.7°C in the preceding charge process was suggested to ensure high radiator surface temperature during discharge. Nallusamy, Sampath, and Velraj [11] tested and simulated batch-wise discharging operation through intermittent hot water withdrawal, different than the typical continuous one, in an effort to maintain the storage outlet temperature at 45°C for heating purpose. These investigations shed light on the significance of considering practical heating needs on optimizing LHTES design and operation.

Furthermore, supercooling and phase separation problems in using incongruent-melting salt hydrates for latent heat storage have been addressed as another operational issue. Zhao and Wang [12] point out in a perspective study the importance of quantitatively evaluating storage performance affected by these two problems for residential heating applications. Waser,

Maranda, Stamatiou, Zaglio, and Worlitschek [13] incorporated supercooling effect by introduction of a crystallization probability function in the numerical model of a commercial latent heat storage unit designed for domestic heating purpose. According to the authors, this numerical model can accurately predict storage outlet temperature at different heat transfer fluid inlet temperature boundary conditions.

Yet, in a spectrum of numerical LHTES heat transfer investigations related to residential heating applications, only limited research is available from the engineering perspective with transient charging/discharging heat transfer boundary conditions. This is nonetheless usually the case in practical applications as the heat transfer fluid (HTF) inlet temperature and flowrate vary with control strategy, climatic condition, and working condition of inter-correlated system components.

Some studies underline this issue. For instance, Nallusamy and Velraj [14] developed a one-dimensional porous medium model considering the effect of dynamic outlet temperature from the solar thermal collector connected to the LHTES system; a linear temperature profile at the storage inlet temperature profile is set in the model for evaluating practical charging processes. Riahi, Saman, Bruno, Belusko, and Tay [15] implemented a periodic temperature boundary condition at the storage inlet in a two-dimensional LHTES heat transfer model to investigate the effectiveness of such a heat transfer enhancement measure. Wang, Yang, Xiong, Li, and Shah [16] coupled a numerical model of residential solar thermal collectors with a three-dimensional LHTES heat transfer model, where transient solar radiation variation was taken into accounts in boundary condition settings. Li, Zhang, and Ding [17] set transient temperature boundary conditions at the LHTES inlet in a one-dimensional packed bed LHTES model considering thermal response from a heat pump condenser for a charging process in a residential heating system. These numerical studies are founded on the engineering point of view when building HTF heat transfer models and performing simulation.

However, some limitations can be still found in available literature on the topic. First, few studies like [10] set sight on discharge (i.e. coupling LHTES model with heating terminal device model), which is usually the bottleneck of LHTES cycling in a peak load shifting installation mostly due to short available time. Second, transient HTF flow strategies in LHTES have been scarcely investigated. Dynamic HTF flowrate profiles can be used for manipulating charging/discharging rates and HTF outlet temperatures. Such analyses are mostly on TES related to concentrating solar power applications (e.g. [18]) but few are for residential heating applications.

Last, the numerical heat transfer investigations based on macro-encapsulated configuration usually conduct capsule geometry analyses to optimize storage performance, e.g. accelerating charge/discharge by reducing the diameter of the modelled cylindrical or spherical capsules. Yet, the majority of such studies fail to consider the impacts of capsule diameter reduction on storage interior packing conditions. For instance, Regin, Solanki, and Saini [6] evaluate storage performance using spherical capsules with a radius ranging from 20 mm to 60 mm in a cylindrical vessel while keeping the void fraction constant at 0.4. Similarly, Pakrouh, Hosseini, Ranjbar, and Bahrampoury [19] use a fixed void fraction of 0.36 for spherical diameters ranging between 10 and 60 mm, and Wu, Xu, and He et al. [20] use 0.25 for spherical diameters of 0.02 m to 0.1 m. Additionally, Peng, Dong, and Ling [21], Raul, Jain, Gaikwad, and Saha [22], and Pirasaci, Wickramaratne, Moloney, Goswami, and Stefanakos [23] practice the same treatment of using a fixed void fraction for different capsule dimensions, which may lead to inaccurate prediction of the total PCM volume and thereby heat storage capacity in the storage unit.

Addressing these gaps, in this work, we developed and validated a numerical LHTES heat transfer model for thermal performance evaluation and control strategy optimization. Transient storage inlet boundary conditions were implemented for both HTF temperature and flowrate in discharging performance simulation considering actual storage working conditions. The

modelled LHTES prototype was previously designed and tested for integration in residential heating systems; however, the experimental characterization results infer that the design and operation of such a prototype, if kept in status quo as displayed in the authors' previous work [24], is unlikely to perform desirably for load shift. Therefore, the objective of this study is twofold. Step one, improved storage design and operational strategy were proposed for the prototype to fulfil the defined discharging performance requirement. Step two, through presenting the entire storage performance evaluation and optimization approach, we provide better engineering understanding in the design phase and a control optimization approach in the operational phase for LHTES aimed at residential heat load shifting.

2. Background

The optimization analysis calls for considerations in fundamentals of residential heating design and operation. These considerations and the prototype thermal performance are briefed in this section.

2.1 Residential heating application

In Swedish dwellings without district heating network connection, heat pumps have vastly replaced boilers for heat generation [25] and hydronic radiators are the most common heating terminal device [26]. In Fig. 1(a), an example of single-family heat pump heating system design is provided: the condenser is connected to the hydronic radiator system for space heating while the installation of a desuperheater, which can be found in some commercial heat pump units, is for producing domestic hot water (DHW). A three-way mixing valve can be either installed at the radiator forward point, as displayed in Fig. 1(a), or at the return point to control the radiator forward/return temperatures.

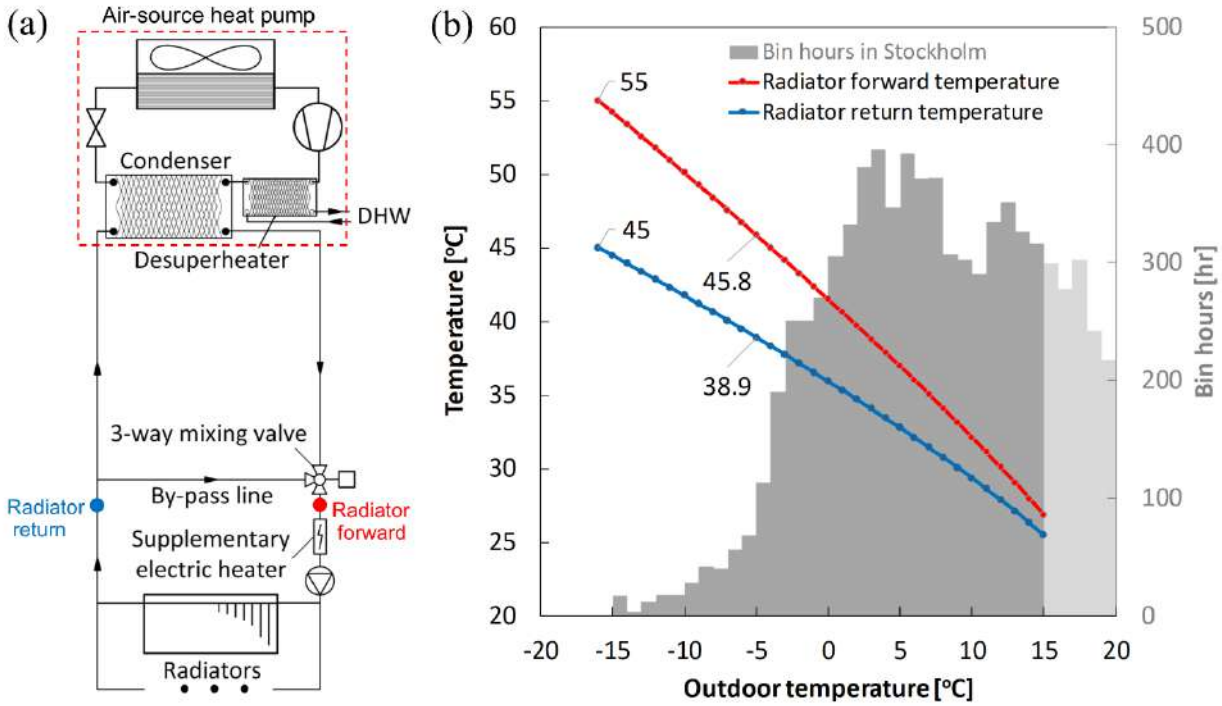

Fig. 1 An example of design and control of a single-family heat pump heating system in Sweden: (a) simplified heating system layout with an air-source heat pump simultaneously covering space heating and domestic hot water (DHW) demands; (b) Typical heat curve controlled radiator forward and return temperatures and bin hours under climatic conditions in Stockholm.

In a typical heating system control, radiator forward and return temperatures are set to increase with decreased outdoor temperatures for combating larger building heat loss [27]; the water circulating flowrate in the hydronic radiator system is typically set constant over various outdoor and forward/return temperatures. According to Swedish building regulations [28], radiator forward/return temperature is commonly set as 55°C/45°C at the design outdoor temperature of radiator systems, which is -16°C for Stockholm. Fig. 1(b) displays an example of outdoor temperature-dependent control curve of radiator forward/return temperatures with a design outdoor temperature of -16°C, together with an annual bin hour distribution in Stockholm. The design outdoor temperature is an extreme condition that barely occurs; the outdoor temperatures above -5°C take up 95% of the total number of heating-season bin hours (-16°C to 15°C). At an outdoor temperature of -5°C, the radiator forward/return temperature is set as 45.8°C/38.9°C. These fundamental information is important for designing LHTES integration into an established heating system without altering the original operating scheme.

In such a heating system, a conceptual plan of TES integration and load shift operation is proposed in Fig. 2. In the charge mode (see Fig. 2a), part of hot water produced in the condenser is directed to the storage. After exchanging heat with PCMs, the storage exit water is mixed with the other part of hot water coming from the condenser as well as the radiator return water to be forwarded to the radiators. In the discharge mode (see Fig. 2b) when the heat pump is switched off, radiator return water is partially directed to the storage for heat retrieval, and the three-valve mixing valve can be controlled to mix warm storage outlet water with the other part of radiator return water passing through the by-pass line with a specific proportion to maintain a desired radiator forward temperature as plotted in Fig. 1(b) for various outdoor temperatures. On top of this discharging scheme, the flow distribution between the storage and by-pass line needs to follow a tuned time-varying profile to handle the non-linear temperature decrease at the LHTES outlet. On the other hand, the LHTES inlet temperature (radiator return temperature) varies with radiator performance variation due to change in the forward temperature. Here, the time variations in both the HTF flowrate and inlet temperature are considered in performance modelling for discharge to reflect actual conditions.

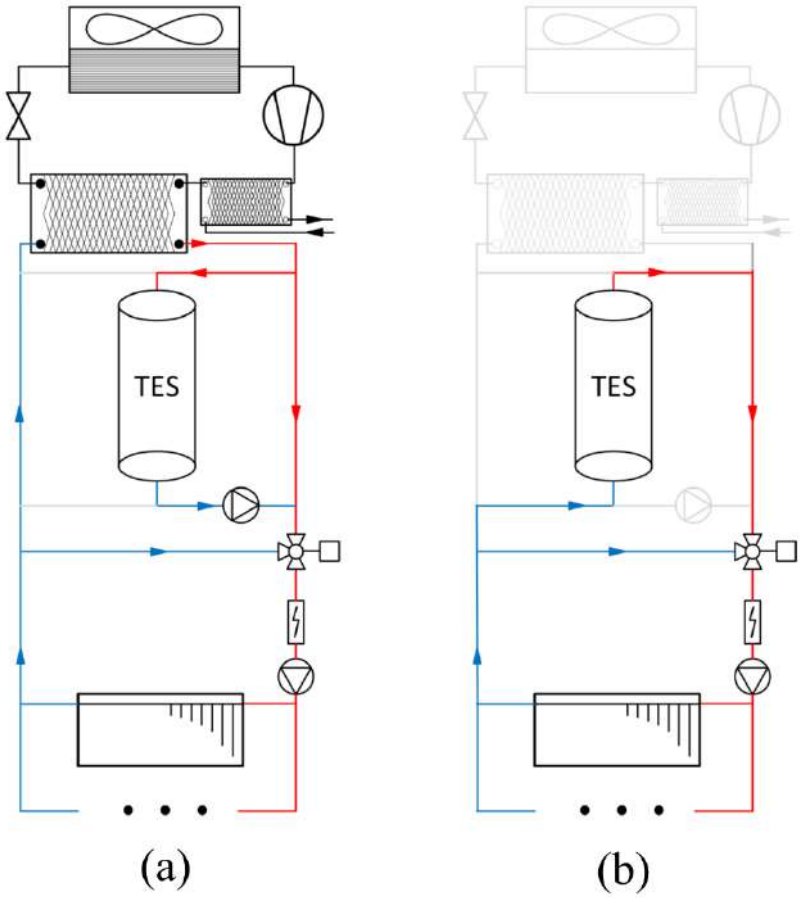

Fig. 2 TES integrating layout and operating strategies in a heat pump heating system: (a) charge mode; (b) discharge mode.

The second consideration in LHTES optimization is on the available time for charge and discharge. According to a recent work on optimizing heat load shifting strategies in Swedish dwellings [29], a charging/discharging timespan of 6 hrs/3 hrs is proposed for maximizing economic savings based on the local electricity retail pricing system. This suggestion on charging/discharging timespan is taken for the analysis in this work.

2.2 LHTES prototype design and performance

From the authors' previous work [24], a benchmarking LHTES prototype based on cylindrically encapsulated PCM was developed and the prototype design is displayed in Fig. 3. The tested PCM is a commercial product, Climsel C58 [30], which has a nominal melting point of 58°C. In the prototype, the central chamber is packed with cylindrical capsules at a maximum loadable amount of 50; voids formed between capsules and are filled with HTF which exchanges heat with PCM (see Fig. 3d). In the central chamber, the packing condition can be characterized by a void fraction (ε) of 0.339, which is the ratio of the void volume to the total central chamber volume.

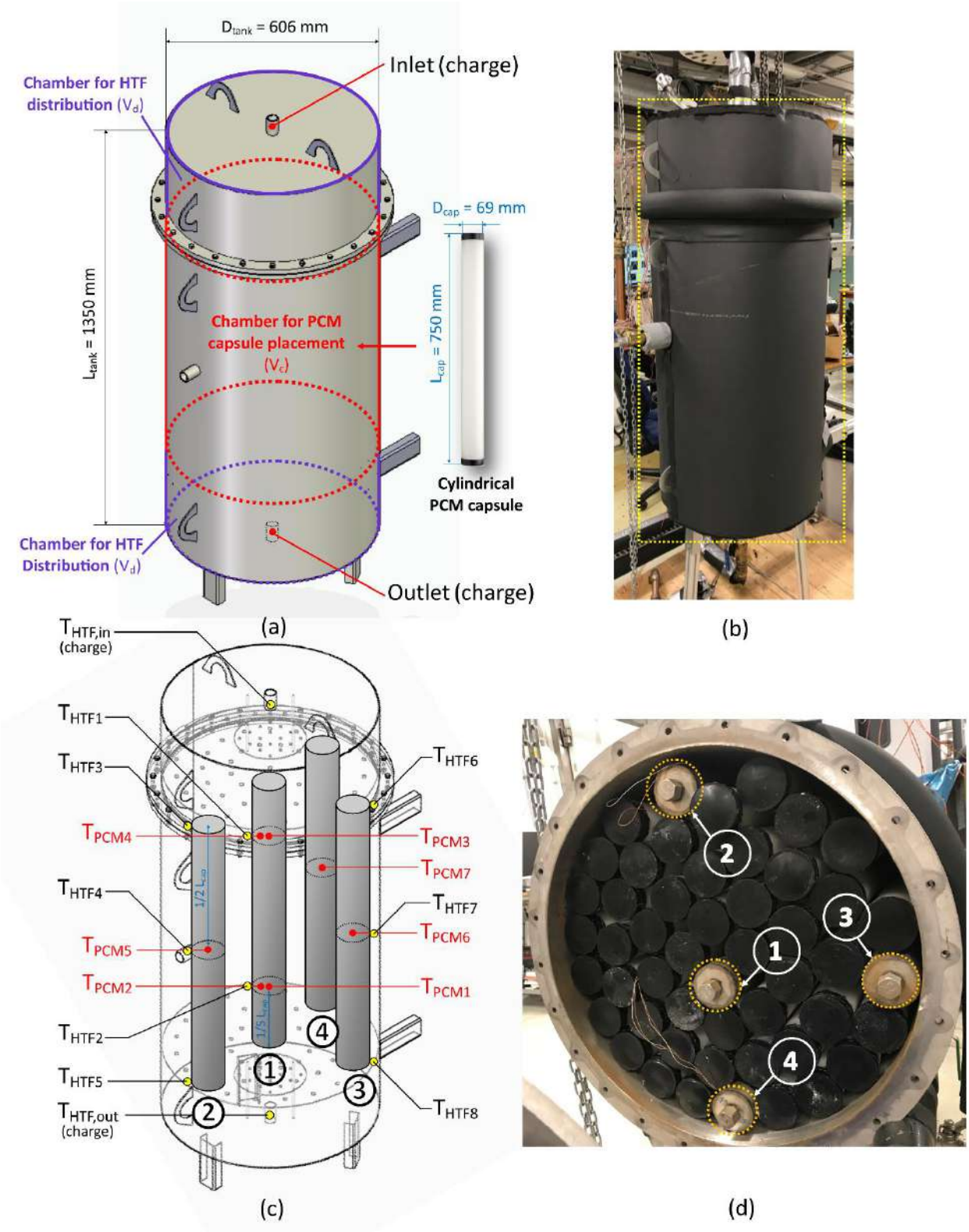

Fig. 3 LHTES prototype with cylindrically encapsulated PCM: (a) design schematic; (b) physical prototype; (c) temperature measuring points for PCM and HTF; (d) cross-section of the packed cylindrical capsules.

The experimental results of the prototype, however, indicate that the discharging thermal behavior cannot fulfil the abovementioned performance criteria as a plug-in unit for integration. Fig. 4 displays the experimental evolutions of storage outlet temperature (T_{out}) and average

PCM temperature (T_{PCM}) in the tank over various discharge processes with different HTF inlet temperatures (T_{in}) and flowrates (V_f). In experiments, the completion time of discharge was determined as the moment when the temperature difference between T_{in} and T_{out} starts to level off. The levelled-off temperature difference was mainly attributed from the storage heat loss and negatively correlated to V_f (0.30 K at 0.25 m^3/h and 0.05 K at 4.0 m^3/h).

With an operating temperature of 45°C to 65°C, the completion time of discharge can only be shortened to around 6 hrs despite increasing V_f from 0.25 m^3/h to 4.0 m^3/h (the latter is already several times higher than the circulating flowrate in a hydronic radiator system for a single-family house). Even when T_{in} was decreased to 35°C (corresponding to radiator return temperature at an outdoor temperature of 2°C), the completion discharge time was more than 4 hrs. Furthermore, with higher HTF flowrate, T_{out} significantly decreased below a usable level for indoor heating (e.g. 55°C) within short time due to increased HTF change rate, as can be observed from dashed curves in Fig. 4. On the other hand, with a fixed HTF flowrate throughout discharging processes, the evolutions of T_{out} indicate non-linear behavior. These experimental observations provide motivations for storage optimization regarding accelerating charge/discharge speed and improving usefulness of the discharged heat.

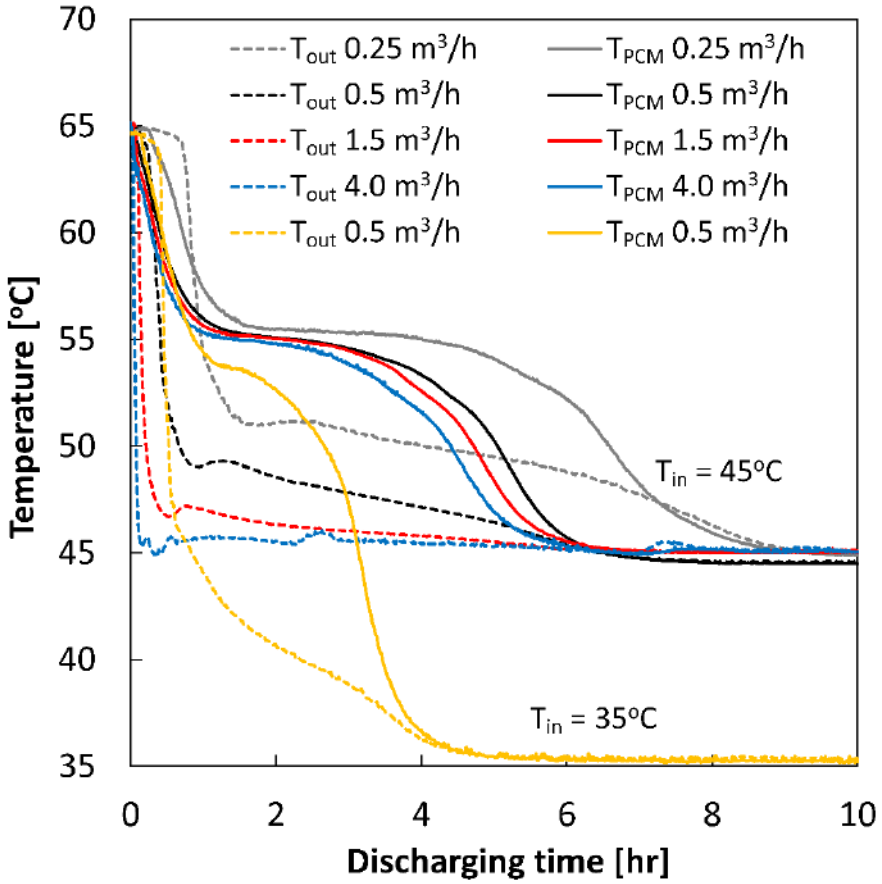

Fig. 4 Experimental results of storage outlet temperature (T_{out}) and average PCM temperature (T_{PCM}) of the prototype under different HTF temperature and flowrate boundary conditions.

3. Modelling Methodology

3.1 LHTES heat transfer model

A finite element method (FEM) based commercial software, COMSOL Multiphysics® 5.4 [31], is used for the numerical studies. Based on the prototype configurations in Fig. 3, a longitudinal axisymmetric cut-plane through a cylindrical PCM capsule is taken as the computational domain. This two-dimensional domain, as illustrated in Fig. 5(a) and (b), represents the overall phase-change heat transfer conditions in the prototype because the HTF

temperature distribution was uniform around PCM cylinders at every longitudinal position thanks to thermal stratification as validated by experimental observations. In addition, air takes up 12% of the volume (92 mm in height) inside capsules for handling PCM thermal expansion.

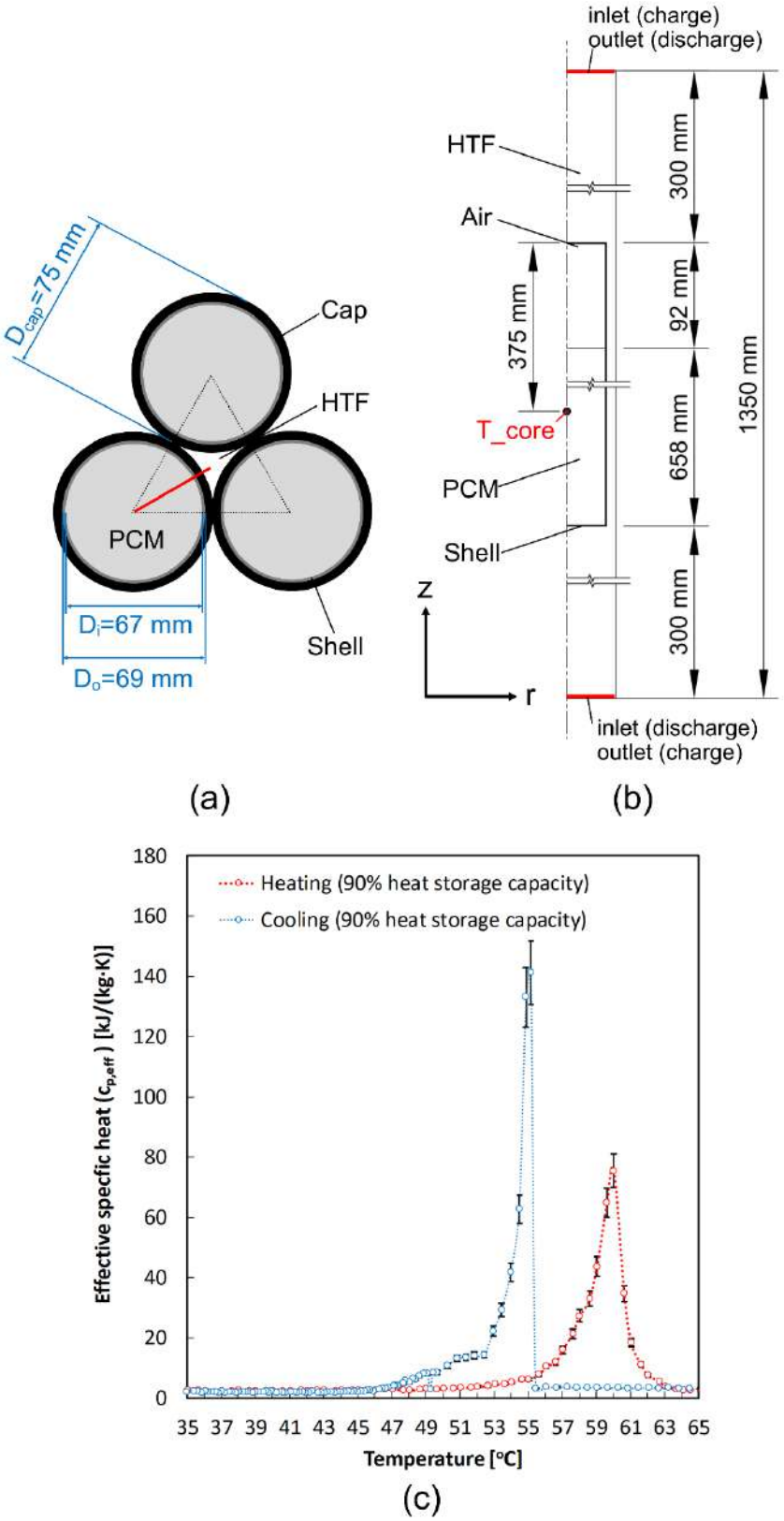

Fig. 5 Model illustration: (a) cross-sectional view of a representative PCM capsule segment (the cut-plane is shown in red); (b) two-dimensional axisymmetric computational domain in cylindrical

coordinates; (c) PCM effective specific heat profiles for heating and cooling (with an expanded uncertainty of ± 6%).

In the material property settings for C58, the macro-encapsulated phase equilibrium behavior observed from experiment was considered. The behavior included: (1) phase separation occurred in the encapsulated C58, leading to around 10% heat storage capacity loss after cycling; (2) negligible supercooling (1 K) was measured in the encapsulated C58 in contrast to the 10 K supercooling measured in temperature-history test [32]. To represent such phase-transition behavior of C58 in actual working conditions, a temperature-dependent profile of effective specific heat ($c_{p,eff}$) was defined in the model as displayed in Fig. 5(c). Here, the melting/freezing enthalpy change determined from T-history tests was incorporated in the $c_{p,eff}$-profile within the phase-transition region with adaptations considering 10% heat storage capacity loss and zero supercooling. Outside phase-transition region, $c_{p,eff}$ equals to solid or liquid specific heat of C58. Other material thermo-physical property inputs for C58 are provided in Table 1.

Table 1 Thermo-physical properties of Climsel C58 [30].

Parameters	**Value**
Phase-change temperature range [°C]	57-61 (melting); 55-50 (freezing)
Latent heat of fusion [kJ/kg]	213
Density [kg/m^3]	1400
Thermal conductivity: solid [W/(m·K)]	0.57
Thermal conductivity: liquid [W/(m·K)]	0.47

Governing equations are established by considering mass, momentum, and energy balances over different computational domains related to HTF-PCM heat transfer. For the HTF (water) domain, the density variation due to temperature change is ignored when calculating the velocity field, $\vec{u}$, and the convective heat transfer rate in laminar flow region between HTF and encapsulation at the capsule surface is expressed with a heat source term, q_h; see continuity and energy equations as Eq. (1) and (2) for HTF. Within the gelled PCM domain heat conduction is the only considered heat transfer mechanism and the energy equation is provided as Eq. (3).

$$\nabla \cdot \vec{u} = 0 \tag{1}$$

$$\rho_f c_{p,f} \left(\frac{\partial T_f}{\partial t} + \vec{u} \cdot \nabla \cdot T_f \right) = k_f \nabla^2 \cdot T_f + q_h \tag{2}$$

$$\rho_p c_{p,eff} \frac{\partial T_p}{\partial t} = k_p \nabla^2 \cdot T_p \tag{3}$$

The main assumptions for the governing equations are:

- Heat loss to the ambient is neglected, because the total amount of heat loss is less than 10% compared to total storage capacity and has limited effect on modelled temperature profile;
- The setting of 10% storage capacity reduction is applied for the entire PCM computational domain as an approximation of the phase separation effect;
- Natural convection in liquid PCM is neglected due to gelling;

- In PCM thermo-physical property settings, a linear thermal conductivity profile versus temperature between solidus and liquidus temperatures is assumed while density variation due to temperature change is neglected.

The settings of the initial and boundary conditions are dependent on the known parameters of storage operation in the application. Typical known parameters include HTF inlet temperature (T_{in}), HTF flowrate (V_f), and initial temperature in the storage unit (T_0), and these parameters will be the input to the model. With the known cross-sectional area of the storage tank (A_{cs}), HTF flowrate can be translated into HTF inlet velocity (u_z) according to Eq. (4).

$$u_z = \frac{V_f}{A_{cs}} \tag{4}$$

With these known inputs, the initial and boundary conditions for HTF and PCM domains were set as provided in Table 2. It is noted that boundary conditions of inlet HTF temperature and flowrate can become time-dependent, i.e. $u_z(t)$ and $T_{in}(t)$, when simulating a discharging process with a transient inlet condition dependent on the coupled radiator's performance from an engineering perspective.

Table 2 Initial and boundary condition settings for HTF and PCM domains.

Conditions	**Settings**	
	HTF domain	**PCM domain**
Initial condition	$T_f = T_0; \vec{u} = 0$	$T_p = T_0;$
Boundary condition		
Top surface ($z = 1350\ mm$)	charge: $\vec{u}_z(t) = -V_f(t)/A_{cs}, \vec{u}_r = 0;$	charge: $T_p = T_{in}(t);$
	discharge: $\partial\vec{u}_z/\partial z = 0, \vec{u}_r = 0$	discharge: $\partial T_p/\partial z = 0$
Bottom surface ($z = 0\ mm$)	charge: $\partial\vec{u}_z/\partial z = 0, \vec{u}_r = 0$	charge: $\partial T_p/\partial z = 0;$
	discharge: $\vec{u}_z(t) = V_f(t)/A_{cs}, \vec{u}_r = 0$	discharge: $T_p = T_{in}(t)$
Left and right walls	$\vec{u} \cdot \vec{n} = 0$	$\partial T_p/\partial r = 0$

The numerical model calculates the storage outlet temperature (T_{out}) over time, and then the thermal power (P_{tes}) is calculated according to the instant heat balance across the storage; see Eq. (5). With that, the accumulated storage capacity (Q) is derived by integrating P_{tes} over any charge/discharge timespan according to Eq. (6). When the timespan is evaluated from the beginning to completion of a charging/discharging process, the accumulated storage capacity represents the total storage capacity of the storage device.

$$P_{tes} = \rho_f c_{p,f} V_f |T_{in} - T_{out}| \tag{5}$$

$$Q = \int_{t_1}^{t_2} P_{tes}\, dt \tag{6}$$

Furthermore, Reynolds number (Re) is calculated referring to the case of internal duct formed amongst stacked cylinders (Fig. 5a). According to Eq. (7), Re is calculated with density and dynamic viscosity of HTF evaluated at the average temperature of storage inlet and initial temperatures and the average HTF velocity in the duct in the central chamber of the storage tank (u_f). The hydraulic diameter of the HTF channel (D_h) in the prototype design is 17.9 mm.

For the prototype design, *Re* is 762 for the highest tested flowrate (4.0 m^3/h) and 48 for the lowest (0.25 m^3/h) for a capsule outer diameter of 69 mm, indicating laminar flow regime for all evaluated cases.

$$Re = \frac{\rho_f u_f D_h}{\mu_f} \tag{7}$$

State of charge (SoC) of the LHTES unit is defined as the ratio of the accumulated storage capacity supplied to or extracted from the storage within a certain timespan to the total storage capacity at the completion of charge or discharge [33]. SoC can be calculated based on heat balance on the HTF side for a charge/discharge process according to Eq. (8), where t_{comp} stands for the completion time of charge/discharge. The completion time is determined as the moment when the accumulated storage capacity reached 99% of the total capacity in the numerical modelling.

$$SoC = \frac{\int_o^t P_{tes}\, dt}{\int_0^{t_{comp}} P_{tes}\, dt} \tag{8}$$

The two-dimensional domain was discretized with a built-in triangular mesh. The mesh independence analysis was carried out by examining three settings of average mesh quality (0.86, 0.90, and 0.97) and the results showed that the completion time of charge varies up to 2%. The mesh with a quality of 0.86 and element amount at 2091 was selected for presenting the validation results.

Time discretization was realized using backward differentiation formula (BDF) as one of the built-in algorithms in COMSOL Multiphysics® 5.4. The time step was set self-adaptive for minimizing computational time with a convergence criterion of 10^{-3} for all equations at each time integration. With this setting, the time step was increased at most twofold for the next time integration when the local truncation error was 16 times smaller than the tolerance.

To check the time step independency, two sets of simulation with a fixed time step of 1 s and 10 s were performed; accumulated storage capacity during the first six hours of a charging process (T_{in} = 65°C; T_0 = 45°C; V_f = 0.25 m^3/h) was examined as self-adaptive time step method often leads to a higher level of error during the initial charging/discharging period when temperature gradient is high. First, as displayed in Table 3, the difference in accumulated storage capacities between 1 s and 10 s time step simulation is negligible (<0.2%). This implies that a time step of 1 s is small enough for obtaining time step independent simulation results. As compared with the experimental results, fixed time step leads to lower deviation in the simulated accumulated storage capacity after hour 6 (0.2%-0.3%) than the self-adaptive time step (1.9%). Using 10 s time step can improve 1.7% modelling accuracy in accumulated storage capacity relative to the self-adaptive time step, however requiring 26 longer computational time. Considering the low error level and high computational efficiency, the self-adaptive time step was used for further simulation in this work.

Table 3 Accumulated storage capacity and computational time with different time step settings.

Time step setting		**Accumulated storage capacity after hour 6 [kJ] (relative difference to experiment)**	**Computational time [hrs][a]**
Fixed time step	1 s	46497.8 (0.3%)	82.5
	10 s	46422.5 (0.2%)	8.0

Self-adaptive time step	47214.8 (1.9%)	0.3
Experiment	46348.0	-

[a] Computed with Intel (R) Core(TM) i7-6600U CPU with 2.60 GHz and a physical memory (RAM) of 16 GB.

3.2 Hydronic radiator model

As explained in Section 2.1, during a discharging process when the heat pump is switched off, the LHTES is in serial connection with the hydronic radiator system to provide heating. Hence, the storage inlet temperature (T_{in}) equals to the radiator return temperature (T_r), which is affected by the radiator thermal performance in terms of the radiator forward temperature (T_f) and radiator heating power (P_{rad}). To determine the radiator behavior, log mean temperature difference (*LMTD*) method can be used assuming a quasi-steady state condition in the radiator for each evaluation per time step [34]. According to the mixing configuration with a by-pass line in which the water is defined as V_{by}, the radiator forward temperature derived from heat balance at the mixing point according to Eq. (9) and (10). An illustration of temperature and flowrate conditions of water is provided in Fig. 6 for a discharging process where LHTES releases heat to the radiators.

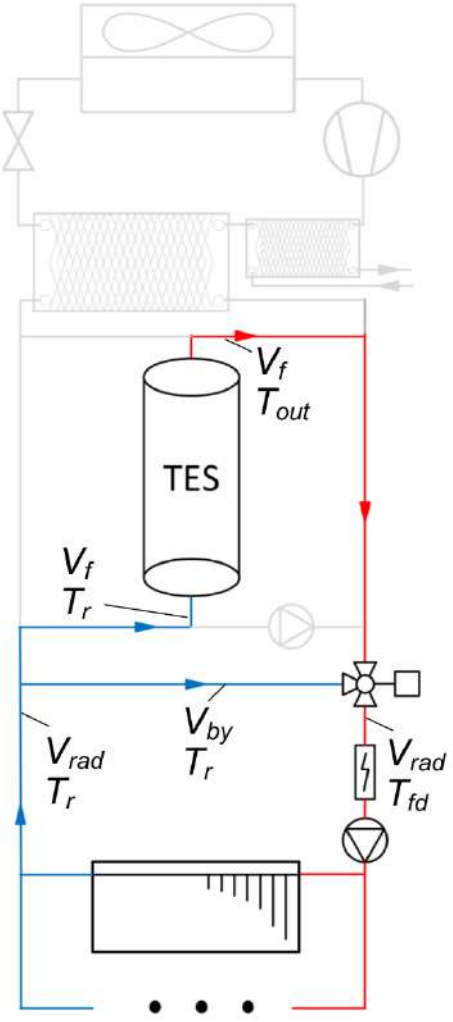

Fig. 6 Illustration of temperature and flowrate conditions of water in a discharging process.

$$\rho_f c_{p,f}\left(V_f T_{out} + V_{by} T_r\right) = \rho_f c_{p,f} V_{rad} T_f \quad (9)$$

$$V_{by} = V_{rad} - V_f \quad (10)$$

Then, iteration was performed to deduce T_{fd} and T_r by matching P_{rad} calculated by two sets of equations, heat balance on the water side with Eq. (11) and *LMTD* heat exchanger analysis with Eq. (12) and (13), to determine the temperature profile of the radiator for a given indoor temperature (T_{room}) and a specific radiator design in terms of the water circulating flowrate (V_{rad}) and overall heat transfer coefficient (UA_{rad}). In Eq. (12), a stands for a radiator exponent which usually ranges between 1.2 and 1.3 [34] and it was set to 1.25 in this work.

$$P_{rad1} = \rho_f c_{p,f} V_{rad} (T_{fd} - T_r) \quad (11)$$

$$P_{rad2} = UA_{rad} \cdot LMTD^a \quad (12)$$

$$LMTD = \frac{(T_{fd} - T_{room}) - (T_r - T_{room})}{\ln\left(\frac{T_{fd} - T_{room}}{T_r - T_{room}}\right)} \quad (13)$$

In this work, a typical single-family house in Sweden built in 1960s was chosen to create a specific working environment representing a practical application environment for LHTES operation. On this dwelling, parameters for simplified heating load calculation and radiator design information are provided in Table 4; the total UA-value of the hydronic radiator system was calculated as 0.14 kW/K to maintain indoor thermal comfort. The dwelling has a heating load of 9.6 kW at the design outdoor temperature of -16°C and 6.7 kW at -5°C. In optimization analysis, this typical residential heating context will be used to set criteria for the desired charging/discharging performance.

Table 4 Heating load and radiator design of a typical single-family house in Sweden [35].

Parameters	**Value**
Building	
Living area [m^2]	160
Total UA-value of building envelope (including wall, floor, roof and window) [kW/K]	0.17
Building ventilation heat loss coefficient [kW/K]	0.08
Building infiltration heat loss coefficient [kW/K]	0.02
Indoor thermal comfort temperature (T_{room}) [°C]	20
Heating load at design outdoor temperature [kW]	9.61
Radiator	
Radiator model	Panel type with DC01 Carbon Steel
Total UA value of the hydronic radiator system (UA_{rad}) [kW/K]	0.14
Designed water circulating flowrate (V_{rad}) [m^3/h]	0.84

3.3 Transient boundary condition for LHTES model

Throughout a discharging process in an integrated heating system, T_{out} generally decreases with the proceeding of the state of charge in LHTES, thus leading to decrease in T_{fd} as well as T_r and eventually T_{in} due to coupling. To depict this thermal response from the radiators in LHTES heat transfer simulation, an interface between the LHTES and radiator model was developed. The coupled computational procedure is displayed in Fig. 7. At each time step of LHTES heat transfer simulation, T_{in} took the value of T_r calculated from the iterative radiator model; the instant HTF flowrate (V_f) was read from a predefined HTF flowrate profile. Accordingly, these updated HTF inlet temperature and flowrate were taken as the updated boundary conditions at the next time step of computation. This calculation approach was designed for allowing LHTES heat transfer simulation to be conducted with transient inlet boundary conditions defined with working conditions in the coupled terminal device, e.g. radiator.

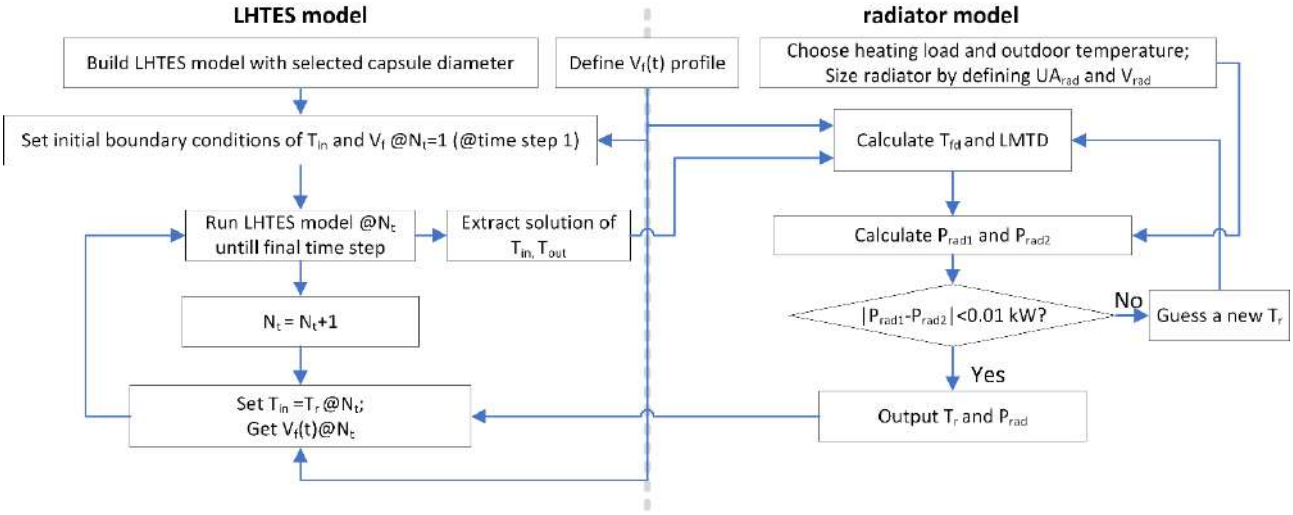

Fig. 7 LHTES heat transfer simulation procedure with transient inlet boundary conditions coupled with radiator thermal performance.

4. Results and Discussion

In this section, the LHTES heat transfer model is first validated with experimental results (Section 4.1) and then employed for analysing the optimization measures of capsule diameter reduction (Section 4.2), time-varying HTF flow strategies (Section 4.3), and storage tank diameter increase (Section 4.4). In Section 4.1 and 4.2, the heat transfer simulation was based on time-constant inlet boundary conditions as the LHTES unit was considered as a standalone component. In Section 4.3 and 4.4, boundary conditions were set as time-varying using the procedure as described in Section 3.3 as the analysis was related to the application of LHTES in a typical residential heating context, which has been defined in Table 4.

4.1 Numerical model validation

The validity of the model was proved by comparing the accumulated storage capacity between the experimental and simulation results. The experimental accumulated storage capacity was determined in a similar post-processing way as simulation: based on Eq. (5) and (6), the capacity was calculated by integrating thermal power deduced from the measured temperature difference across the storage. As displayed in Fig. 8, progressions of the accumulated storage capacity in four charging/discharging processes for both experiment and simulation suggest that the model can accurately predict transient thermal output from the

storage. The relative difference of the capacity between experiment and simulation is within 4% throughout the four evaluated processes.

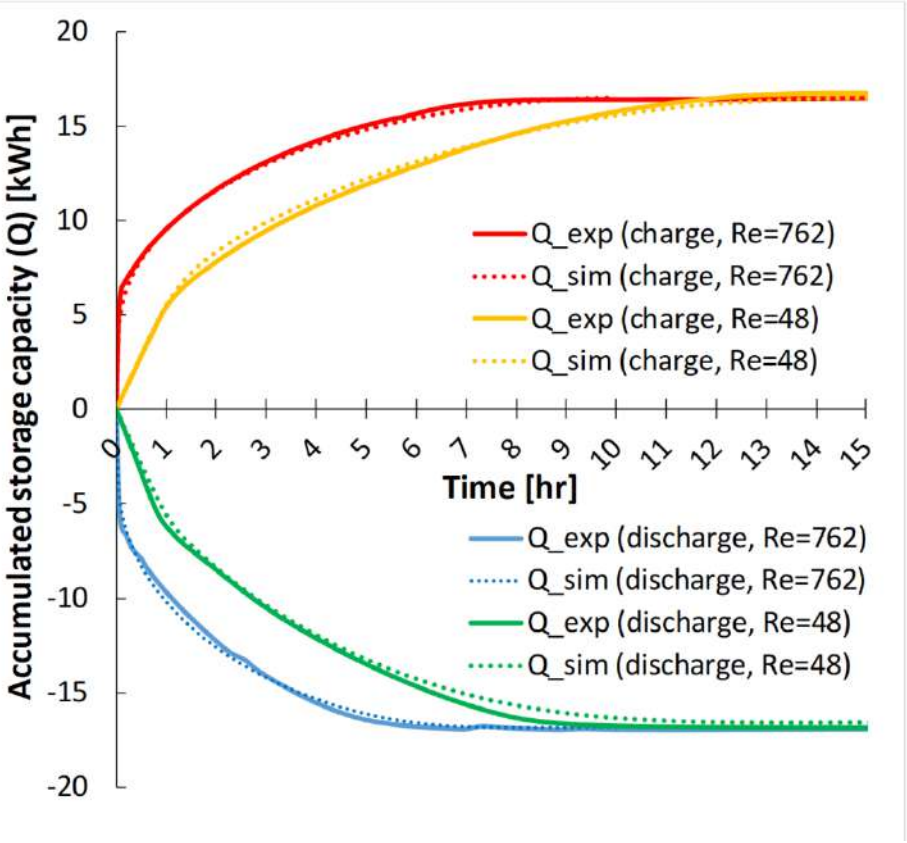

Fig. 8 Experimental vs. simulation results of accumulated storage capacity (Q) for both charge and discharge test conditions with the full HTF flowrate range Re=[48;762] (Q for discharge is expressed in negative values for distinction).

4.2 Capsule diameter effect

One way to achieve more rapid thermal response from the storage is to reduce the T because this decreases the conductive thermal resistance in the PCMs and increases the HTF velocity. Therefore, the objective was set at finding a sufficiently small capsule diameter that allows complete charge/discharge within the given timespan (6 hrs/3 hrs). In doing so, the operating temperature range was fixed at 45ºC to 65ºC corresponding to a design outdoor temperature condition.

When D_o is reduced, the loadable number of the capsules (n) increases and the void fraction (ε) in the central chamber of the tank decreases due to increased ratio between the chamber diameter (D_{tank}) and D_o. An illustration of packing conditions is provided in Fig. 9: the packing condition becomes more compact when D_o is reduced from 69 mm, the prototype capsule diameter, to 25 mm, as ε decreases from 34% to 27% and the number of capsules increases from 50 to 422.

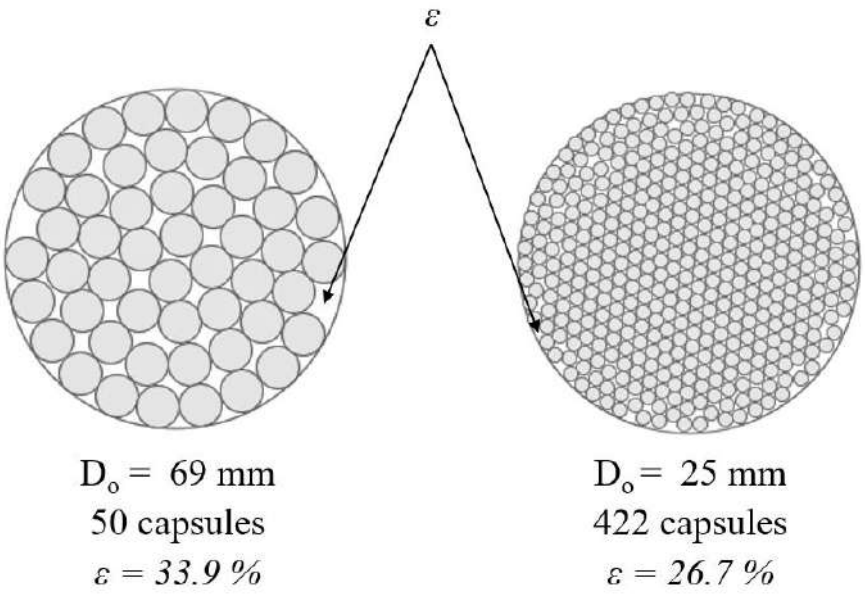

Fig. 9 Packing conditions with two different capsule outer diameters (69 and 25 mm).

When packing the tank with a capsule outer diameter ranging from 65 mm to 15 mm, void fraction exhibits a generally decreasing trend due to geometrical phenomena related to the densest packing solution. Moreover, the capsule number increases in a non-linear manner. The variations of these parameters with varying D_o are displayed in Fig. 10(a). Change in the void fraction also impacts the distribution of volumes of HTF, PCM and capsule shell in the central chamber. The total volume of the central chamber remains unchanged but as the capsule diameter decreases and the number of capsules increases, the volume of capsule shell increases (shell thickness of 1 mm), as displayed in Fig. 10(b). Therefore, despite 8% reduction in the void fraction from 69 mm to 15 mm, the total PCM volume decreases by 11% in large part owing to capsule shell volume increasing from 8 L to 39 L (shell thickness was kept as 1 mm).

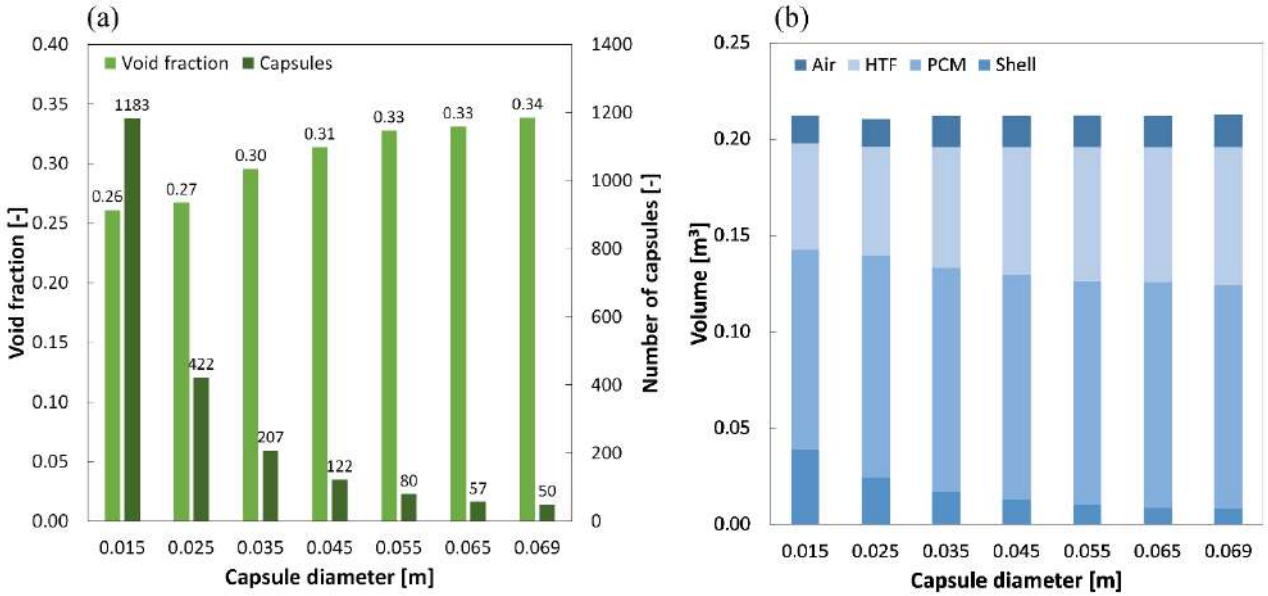

Fig. 10 Configurations in the storage central chamber with different capsule diameters: (a) void fraction and number of capsules; (b) volume distribution of PCM, air, HTF, and capsule shell.

With the developed model, the effect of diameter reduction on total thermal energy storage capacity (Q) and completion time of charge and discharge are analysed. The simulation results show that the complete charging time was 12.5 hrs when HTF flowrate was set at 0.25 m^3/h at

D_o of 69 mm, which was validated by the experimental results (12.3 hrs) with a relative difference of 2%. The numerical model was then used to simulate the effect of capsule diameter reduction, from 65 mm to 15 mm with a 10 mm step size. As shown in Fig. 11(a), it is possible to reduce the completion time for both charge and discharge by decreasing capsule diameter. For charge, the completion time can be shortened to 5.2 hrs (58%) when decreasing D_o from 69 mm to 15 mm. The same time reduction effect was modelled for discharge: the complete discharging time can be cut from 9.8 hrs to 3.0 hrs by 70%. With the capsule outer diameter reduced to 15 mm, the completion time requirement can be met for both charge and discharge at the design outdoor condition.

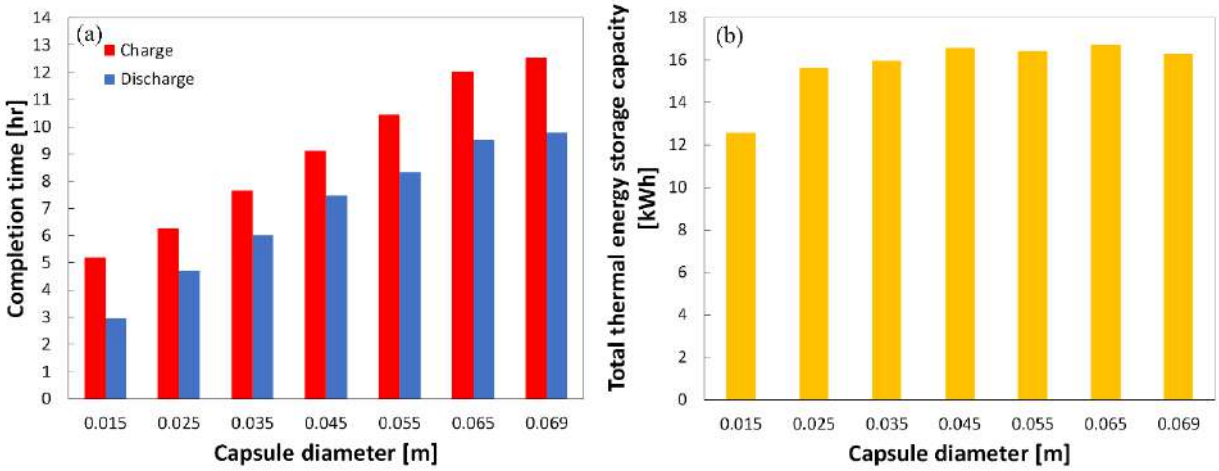

Fig. 11 Storage thermal performance with different capsule diameters: (a) completion time of charge and discharge; (b) thermal energy storage capacity (discharge).

In general, the completion time is shorter in discharge than charge, in large part because the temperature difference between the HTF inlet temperature and phase-transition onset temperature in discharge (10 K) is higher than charge (8 K) with the same operating temperature range of 45°C–65°C. This means that the driving force for phase-change heat transfer is larger during discharge. Other possible reasons include 1) solid PCM has a higher thermal conductivity (0.57 W/K) than liquid (0.47 W/K) as indicated by the manufacturer; 2) heat loss is slightly larger during charge because of the higher operation temperature in storage.

The variation in the volume distribution among HTF, PCM, air, and capsule shell with different capsule diameters influences the total thermal energy storage capacity. As shown in Fig. 11(b), when D_o is reduced to from 69 mm to 15 mm, a 23% drop in the storage capacity is found (Q decreases from 16.3 kWh to 12.6 kWh). This behavior is mainly caused by the significant increase in the capsule shell volume and thus the decrease in both PCM and water volumes as shown in Fig. 10(b).

4.3 HTF Flowrate profiling during discharge

As explained in Section 2.2, maintaining radiator forward temperature is an important operational requirement. This requirement can be potentially achieved through tuning the flowrate allocation between the storage outlet and by-pass line with the three-way mixing valve. Based on the optimized capsule outer diameter (15 mm) allowing time-efficient charge/discharge, the control optimization of storage is investigated by comparing different HTF flowrate (V_f) profiles throughout a 3-hr discharging process, aimed at providing stabilized radiator forward temperature for the entire period according to the heat curve as shown in Fig. 1(b). In this section, the evaluation is performed for a specific condition when the outdoor temperature equals -5°C; hence the storage inlet temperature at the first time step was set as

38.9°C, the radiator return temperature at this outdoor temperature. The desired radiator forward temperature is 45.8°C.

In doing so, five different HTF flow strategies were designed and investigated on the effectiveness of handling the non-linear temperature behavior at the storage outlet. The five profiles, namely Case 0–4, are displayed in Fig. 12. Except from Case 0 where a baseline profile was established with a time-constant V_f value of 0.22 m^3/h, the other four profiles (Case 1–4) were designed with time-increasing flowrate profiles in an effort to offset the effect from decreasing temperature difference in discharge. Furthermore, Case 2–4 were designed in a way that V_f increases after 0.83 hr because it is the moment when the storage outlet temperature starts to significantly fall due to the completion of HTF volume replacement in the tank. In addition, a parabolic profile was specially adopted (Case 4) in contrast to the other linear profiles.

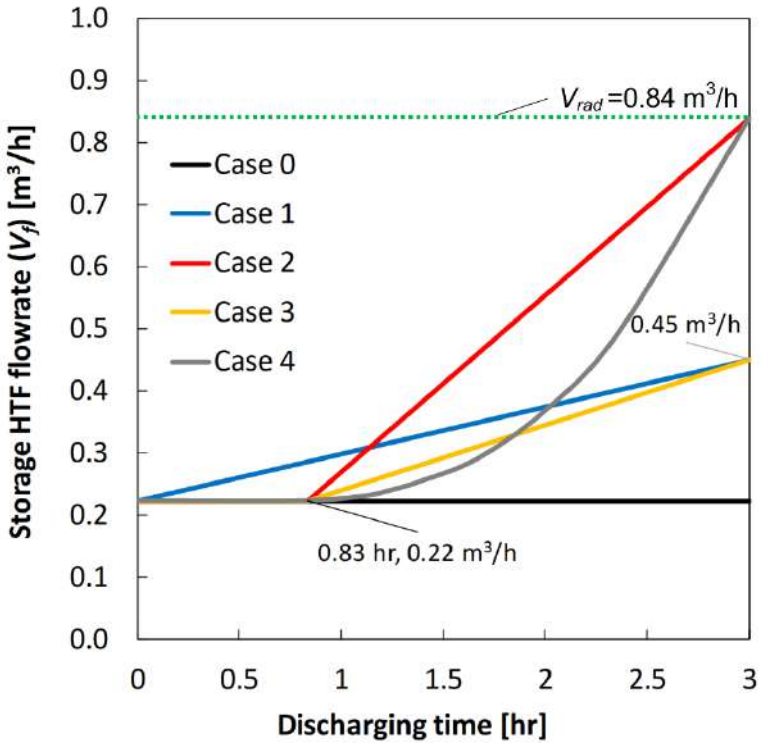

Fig. 12 Investigated HTF flowrate profiles (Case 0-4).

The simulated storage inlet/outlet temperature (T_{in}/T_{out}) and radiator forward temperature (T_f) are plotted in Fig. 13(a) and (b). In Case 0, T_{in} starts to decline after around hour 0.8 and displays a plateau around 55°C, the freezing onset temperature of the PCM, between hour 2 and hour 2.5, followed by a sharp decrease after the completion of freezing. The decrease in T_{in} behaves similarly as in T_{out} in terms of temperature profile shape because the decrease in T_{in} brings down the radiator forward temperature T_{fd} (see Fig. 13b) and accordingly T_{in} when HTF circulates back to the storage. With this time-constant flowrate profile, T_{fd} drops below 45.8°C after around 1 hr.

Differently, in Case 1, the gradual increase in V_f leads to slight rise in T_{fd} above 45.8°C till around hour 0.9 despite T_{out} being constant. This is because the flow in the storage outlet line, where water temperature is warmer, taking a gradually increasing share at the mixing point to the radiator forward line. After hour 0.9, T_{fd} starts to decrease from 49.3°C due to declined T_{out} and drops to 45.8°C at hour 1.6 before stabilization. Accordingly, the similar fluctuation is reflected on the radiator exit behavior in terms of the radiator return temperature (T_r) and consequently T_{in} when water circulates back to the storage, as indicated in Fig. 13(a).

A similar behavior can be found in Case 2 and Case 3: when V_f increases linearly after hour 0.83, T_{fd} increases accordingly above 45.8°C but to different extents between the two cases because of different flowrate increasing rates. In Case 2, the more rapid increase in V_f after hour 0.83 leads to more sharply increased T_{fd} until hour 1.3, countering the decline in T_{out} which lowers the T_{fd} at the mixing point; T_{in} varies similarly as T_{fd}. Last, in Case 4 where a parabolic flowrate profile was adopted, T_{fd} can be stabilized at around 45.8°C for 2.1 hrs because, with this specific profile, the increasing HTF flowrate in the storage outlet can approximately cancel out the effect from the decrease in T_{out} on lowering T_{fd} at mixing. It is inferred from the comparisons shown in Fig. 13(b) that Case 4 outperforms than the other cases for giving a stable radiator forward temperature at the required temperature level.

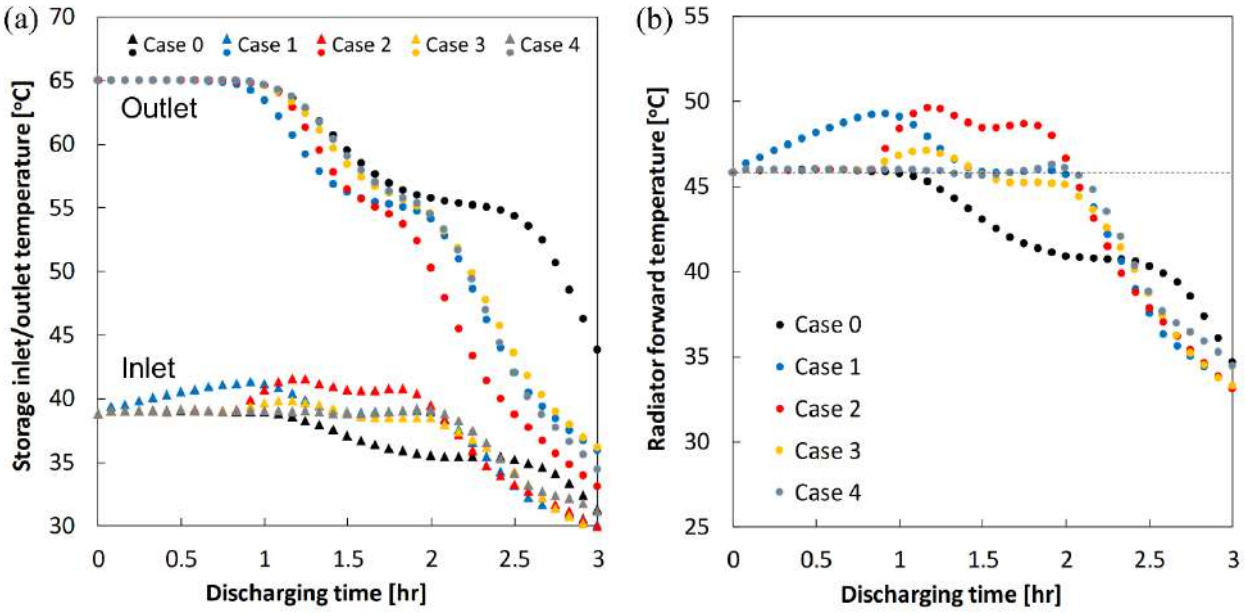

Fig. 13 Discharging temperature evolutions with different HTF flow profiles (Case 0-4): (a) Storage inlet/outlet temperature; (b) radiator forward temperature.

Table 5 provides a summary of the simulated discharge performance with different HTF flowrate profiles. Here, SoC is evaluated according to Eq. (8) for the useful discharge timespan by putting the total thermal energy storage capacity with an operating temperature range of 38.9°C to 65.0°C as the denominator. The comparisons indicate that Case 1, 2, and 4 can provide useful heat for around 2 hrs; the difference in the useful time between these three cases is insignificant, up to 3%. Accordingly, SoC is high (83% to 88%) for these three cases because of the longer timespan for considering the accumulated storage capacity. Compared with the bassline Case 0, using these three profiles can extend the useful discharging period by around 50%.

Table 5 Summary of discharge performance with the five evaluated HTF flowrate profiles.

Parameter	**Case**				
	0	**1**	**2**	**3**	**4**
Feature of HTF flowrate profile	Time-constant[(a)]	Linear increasing[(b)]	Stepwise linear increasing[(b)]	Stepwise linear increasing[(c)]	Stepwise parabolic increasing[(b)]

Time when T_{fd} > 45.8°C [hr]	1.00	1.99	2.04	1.48	2.05
Accumulated storage capacity [kWh]	6.7	14.2	14.7	10.0	13.7
SoC [-]	40%	85%	88%	60%	83%

(a) At 0.22 m^3/h;
(b) From 0.22 m^3/h to 0.84 m^3/h;
(c) From 0.22 m^3/h to 0.45 m^3/h.

Both Case 2 and Case 3 have a stepwise linear flowrate profile. Compared with Case 2, Case 3 shows a lower SoC (60%) and shorter useful discharge time (1.48 hrs), because the more slowly increased HTF flowrate in Case 3 retrieves less amounts of heat capacity (10.0 kWh) than in Case 2 (14.7 kWh), resulting in a lower radiator forward temperature. Case 4 shows a higher SoC and longer useful discharge time than Case 3, too, as the parabolic profile displayed in Fig. 12 can maintain the radiator forward temperature and thereby storage inlet temperature at the required temperature threshold for longer time.

Yet, none of the three cases can provide useful heat for the entire desired discharging period of 3 hrs in large part due to the limited storage capacity with the original prototype vessel design, as the high discharge efficiencies indicate that most of the storage capacity has been released during the first 2 hrs.

4.4 Storage tank diameter increase

According to the preceding analyses, enlarging the storage tank may prolong the useful discharge period to 3 hr for maintaining the radiator forward temperature (T_f) around 45.8°C. To investigate that, LHTES heat transfer simulation was performed for two storage tank designs with the tank inner diameters (D_{tank}) increased to 0.7 m and 0.8 m, respectively, while keeping other dimensions unchanged. For each new tank diameter, a HTF flowrate profile was proposed on a parabolic basis and displayed in Fig. 14 where the evolution of the simulated T_{fd} is also shown. In both cases, the forward temperature requirement is fulfilled; however, the flowrate necessary for T_{fd} to be maintained above 45.8°C after hour 1.5 is higher when D_{tank} is equal to 0.7 m than 0.8 m. The main reason is that, with the latter diameter, the tank volume is 30% larger and therefore HTF volume replacement takes longer time to complete, allowing more sufficient time for HTF to exchange heat with PCM and reaching a higher temperature when exiting the storage.

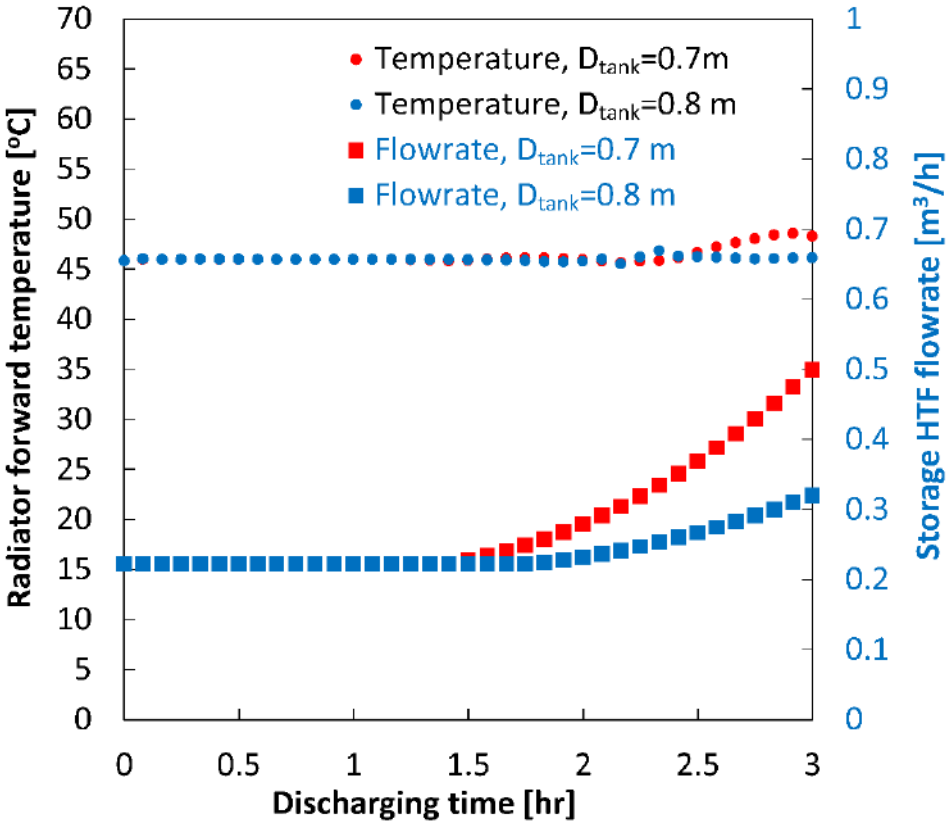

Fig. 14 Radiator forward temperature at increased storage tank diameters with parabolic HTF flowrate profiles.

Yet, the total storage capacities in the two designs are different: the capacity is 23.5 kWh when D_{tank} is equal to 0.7 m and 31.1 kWh at 0.8 m; SoC for this 3-hr operation was calculated to be 86% and 65%, respectively. This indicates that, with a larger tank size, SoC would become lower for the same 3-hr discharging process. On the other hand, the capital investment of the LHTES component would increase due to the increased installation number of 15 mm-diameter PCM capsules (1681 for D_{tank} equal to 0.7 m and 2204 for 0.8 m). The comparison implies a trade-off between the easiness of meeting the radiator heating requirement and use ratio of the heat storage materials during discharge.

5. Conclusion

In this paper, the thermal performance of a cylindrically encapsulated latent heat thermal energy storage prototype is investigated with a numerical heat transfer model. A comprehensive storage performance simulation, evaluation, and optimization approach is presented and used in an effort to make the prototype realize desired load shift function when integrated in a single-family heating system. The analyses in this work give rise to the following conclusions:

(1) Validity of the developed numerical heat transfer model is proved as the relative difference in the accumulated thermal energy storage capacity between the simulation and experimental results is within 4% throughout four charging/discharging processes different in convective heat transfer conditions.

(2) The heat transfer simulation for optimizing the storage design shows that reducing the capsule outer diameter from 69 mm, as in the original prototype design, to 15 mm can shorten the completion charge/discharge time from 12.5 hrs/9.8 hrs to 5.2 hrs/3.0 hrs,

fulfilling the time requirement (6 hrs/3 hrs) defined under optimal load shift strategies. However, such capsule diameter reduction also leads to 23% decrease in the total thermal energy storage capacity due to increased capsule shell volume.

(3) The heat transfer fluid flow strategy analyses indicate that, with a parabolic time-increasing flowrate profile, the useful discharge time can be extended to around 2 hrs from 1 hr when using a time-constant flowrate profile. With the parabolic profile, the radiator forward temperature can be maintained around 45.8°C during the useful discharge period to ensure indoor thermal comfort at an outdoor temperature of -5°C.

(4) Increasing the storage vessel diameter from 0.6 m is to 0.7 m and to 0.8 m can help sustain useful discharge timespan to 3 hrs as required by recommended on-peak load shifting duration. Yet the state of charge decreases with the further enlargement to 0.8 m resulted from increased unexploited storage capacity during the 3-hr discharge.

(5) From the thermal performance simulation and optimization, an improved storage design and operating solution is proposed as to 1) reduce the capsule outer diameter to 15 mm from 69 mm, 2) increase the storage tank size to 0.7 m from 0.6 m, and 3) adopt a parabolic time-increasing heat transfer fluid flowrate profile instead of a time-constant one for a 3-hr discharging process in terms of storage operation. This storage solution can fulfil the desired peak load shifting needs for the majority of heating-season hours if integrated in typical single-family heating system in Sweden.

The discussions in this work have been mainly for a specific residential heating application in Sweden. Yet, the performance evaluation and optimization approach presented in this work can be extended to other types of heating systems with different heating terminal device, system designs and control methods by changing the user demand criteria and the terminal device models coupled with the numerical heat transfer model. Future studies will be carried out on validating the optimized storage design and operational strategy in a field test, as well as on investigating the effectiveness of these measures in an annual load shift analysis.

Acknowledgement

Tianhao Xu would like to thank the Chinese Scholarship Council (CSC) for providing the PhD stipend. The EffsysEXPAND P20 project (funded by Swedish Energy Agency, grant number P40935-1) and the PUMPHEAT project (funded by EU Horizon 2020, grant number 764706) are acknowledged for the financial supports.

References

[1] J. Kensby, A. Trüschel, and J.-O. Dalenbäck, "Potential of residential buildings as thermal energy storage in district heating systems – Results from a pilot test," *Applied Energy*, vol. 137, pp. 773-781, 2015/01/01/ 2015.

[2] J. Pereira da Cunha and P. Eames, "Thermal energy storage for low and medium temperature applications using phase change materials – A review," *Applied Energy*, vol. 177, pp. 227-238, 2016/09/01/ 2016.

[3] G. Diarce, I. Gandarias, Á. Campos-Celador, A. García-Romero, and U. J. Griesser, "Eutectic mixtures of sugar alcohols for thermal energy storage in the 50–90°C temperature range," *Solar Energy Materials and Solar Cells*, vol. 134, pp. 215-226, 2015.

[4] P. Zhang, Z. N. Meng, H. Zhu, Y. L. Wang, and S. P. Peng, "Melting heat transfer characteristics of a composite phase change material fabricated by paraffin and metal foam," *Applied Energy,* vol. 185, pp. 1971-1983, 2017.
[5] T. Nuytten, P. Moreno, D. Vanhoudt, L. Jespers, A. Solé, and L. Cabeza, "Comparative analysis of latent thermal energy storage tanks for micro-CHP systems," *Applied Thermal Engineering,* vol. 59, no. 1-2, pp. 542-549, 2013.
[6] A. Felix Regin, S. C. Solanki, and J. S. Saini, "An analysis of a packed bed latent heat thermal energy storage system using PCM capsules: Numerical investigation," *Renewable Energy,* vol. 34, no. 7, pp. 1765-1773, 2009.
[7] A. de Gracia, E. Oró, M. M. Farid, and L. F. Cabeza, "Thermal analysis of including phase change material in a domestic hot water cylinder," *Applied Thermal Engineering,* vol. 31, no. 17, pp. 3938-3945, 2011/12/01/ 2011.
[8] M. M. Prieto, I. Suárez, and B. González, "Analysis of the thermal performance of flat plate PCM heat exchangers for heating systems," *Applied Thermal Engineering,* vol. 116, pp. 11-23, 2017/04/01/ 2017.
[9] Y. Wang, K. Yu, and X. Ling, "Experimental and modeling study on thermal performance of hydrated salt latent heat thermal energy storage system," *Energy Conversion and Management,* vol. 198, p. 111796, 2019.
[10] F. Agyenim and N. Hewitt, "The development of a finned phase change material (PCM) storage system to take advantage of off-peak electricity tariff for improvement in cost of heat pump operation," *Energy and Buildings,* vol. 42, no. 9, pp. 1552-1560, 9/ 2010.
[11] N. Nallusamy, S. Sampath, and R. Velraj, "Experimental investigation on a combined sensible and latent heat storage system integrated with constant/varying (solar) heat sources," *Renewable Energy,* vol. 32, no. 7, pp. 1206-1227, 6// 2007.
[12] B. C. Zhao and R. Z. Wang, "Perspectives for short-term thermal energy storage using salt hydrates for building heating," *Energy,* vol. 189, p. 116139, 2019/12/15/ 2019.
[13] R. Waser, S. Maranda, A. Stamatiou, M. Zaglio, and J. Worlitschek, "Modeling of solidification including supercooling effects in a fin-tube heat exchanger based latent heat storage," *Solar Energy,* 2018/12/19/ 2018.
[14] N. Nallusamy and R. Velraj, "Numerical and Experimental Investigation on a Combined Sensible and Latent Heat Storage Unit Integrated With Solar Water Heating System," *Journal of Solar Energy Engineering,* vol. 131, no. 4, pp. 041002-041002-8, 2009.
[15] S. Riahi, W. Y. Saman, F. Bruno, M. Belusko, and N. H. S. Tay, "Impact of periodic flow reversal of heat transfer fluid on the melting and solidification processes in a latent heat shell and tube storage system," *Applied Energy,* vol. 191, pp. 276-286, 2017/04/01/ 2017.
[16] Y. Wang, X. Yang, T. Xiong, W. Li, and K. W. Shah, "Performance evaluation approach for solar heat storage systems using phase change material," *Energy and Buildings,* vol. 155, pp. 115-127, 2017.
[17] Y. Li, N. Zhang, and Z. Ding, "Investigation on the energy performance of using air-source heat pump to charge PCM storage tank," *Journal of Energy Storage,* vol. 28, p. 101270, 2020.
[18] K. M. Powell and T. F. Edgar, "Modeling and control of a solar thermal power plant with thermal energy storage," *Chemical Engineering Science,* vol. 71, pp. 138-145, 2012.
[19] R. Pakrouh, M. J. Hosseini, A. A. Ranjbar, and R. Bahrampoury, "Thermodynamic analysis of a packed bed latent heat thermal storage system simulated by an effective packed bed model," *Energy,* vol. 140, pp. 861-878, 2017.

[20] M. Wu, C. Xu, and Y.-L. He, "Dynamic thermal performance analysis of a molten-salt packed-bed thermal energy storage system using PCM capsules," *Applied Energy,* vol. 121, pp. 184-195, 2014.
[21] H. Peng, H. Dong, and X. Ling, "Thermal investigation of PCM-based high temperature thermal energy storage in packed bed," *Energy Conversion and Management,* vol. 81, pp. 420-427, 2014.
[22] A. Raul, M. Jain, S. Gaikwad, and S. K. Saha, "Modelling and experimental study of latent heat thermal energy storage with encapsulated PCMs for solar thermal applications," *Applied Thermal Engineering,* vol. 143, pp. 415-428, 2018.
[23] T. Pirasaci, C. Wickramaratne, F. Moloney, D. Y. Goswami, and E. Stefanakos, "Influence of design on performance of a latent heat storage system at high temperatures," *Applied Energy,* vol. 224, pp. 220-229, 2018.
[24] T. Xu, S. N. Gunasekara, J. N. Chiu, B. Palm, and S. Sawalha, "Thermal behavior of a sodium acetate trihydrate-based PCM: T-history and full-scale tests," *Applied Energy,* vol. 261, p. 114432, 2020/03/01/ 2020.
[25] H. Gadd and S. Werner, "18 - Thermal energy storage systems for district heating and cooling A2 - Cabeza, Luisa F," in *Advances in Thermal Energy Storage Systems*: Woodhead Publishing, 2015, pp. 467-478.
[26] M. Jangsten, J. Kensby, J. O. Dalenbäck, and A. Trüschel, "Survey of radiator temperatures in buildings supplied by district heating," *Energy,* vol. 137, pp. 292-301, 2017/10/15/ 2017.
[27] F. Karlsson and P. Fahlén, "Capacity-controlled ground source heat pumps in hydronic heating systems," *International Journal of Refrigeration,* vol. 30, no. 2, pp. 221-229, 2007/03/01/ 2007.
[28] Boverket´s building regulations – mandatory provisions and general recommendations, 2016.
[29] E. Nyholm, S. Puranik, É. Mata, M. Odenberger, and F. Johnsson, "Demand response potential of electrical space heating in Swedish single-family dwellings," *Building and Environment,* vol. 96, pp. 270-282, 2016.
[30] Climator Sweden AB. *C58 Datasheet*. Available (Accessed 2020-03-31): https://www.climator.com/images/pdf/prodblad_climsel_c58_4.1.pdf
[31] *COMSOL Multiphysics® v. 5.4*. Available (Accessed 2020-03-31): www.comsol.com
[32] Y. Zhang, Y. Jiang, and Y. Jiang, "A simple method, the T-history method, of determining the heat of fusion, specific heat and thermal conductivity of phase-change materials," *Measurement Science and Technology,* vol. 10, no. 3, p. 201, 1999.
[33] G. Zsembinszki, C. Orozco, J. Gasia, T. Barz, J. Emhofer, and L. F. Cabeza, "Evaluation of the State of Charge of a Solid/Liquid Phase Change Material in a Thermal Energy Storage Tank," *Energies,* vol. 13, no. 6, p. 1425, 2020.
[34] F. Karlsson, "Capacity control of residential heat pump heating systems," Doctoral thesis, Department of Building Technology, Chalmers University of Technology, 2007.
[35] M. U. TABULA, "Byggnadstypologier Sverige (In English, Building typologies in Sweden)," TABULA, Mälardalen University, 2009. Available (Accessed 2020-03-31): https://episcope.eu/fileadmin/tabula/public/docs/brochure/SE_TABULA_TypologyBrochure_Mdh.pdf.

Appendix

The appendix provides additional information and data on the modeling procedure for Paper I (the system analysis of integrating the established transient heat transfer model into a multi-family building heating system).

Appendix A illustrates the hourly variation of the multi-family building's heat demand during the week considered in the study.

Appendix B provides additional details on the modeling procedure in IMST-ART of ground-source heat pump for generating a polynomial correlating the COP_1 to the inlet and outlet temperatures of the secondary fluids in the condenser.

Appendix C describes the equation used to calculate the heat losses from the LHTES tank in the building heating system during "idle" hours, i.e. hours when it was not operated.

Appendix D presents the bin hour analysis performed for the electricity prices, showing which hours of the day statistically were "peak" and "valley" hours, respectively.

Appendix E illustrates the data for the carbon dioxide emissions related to the electricity production for the European Union.

Appendix A – Heating demand variations during the week

This appendix aims to give the reader some more insight into the hourly variations of the multi-family building's heating demand during the period simulated in the study in Paper I, i.e. the first week of January 2019.

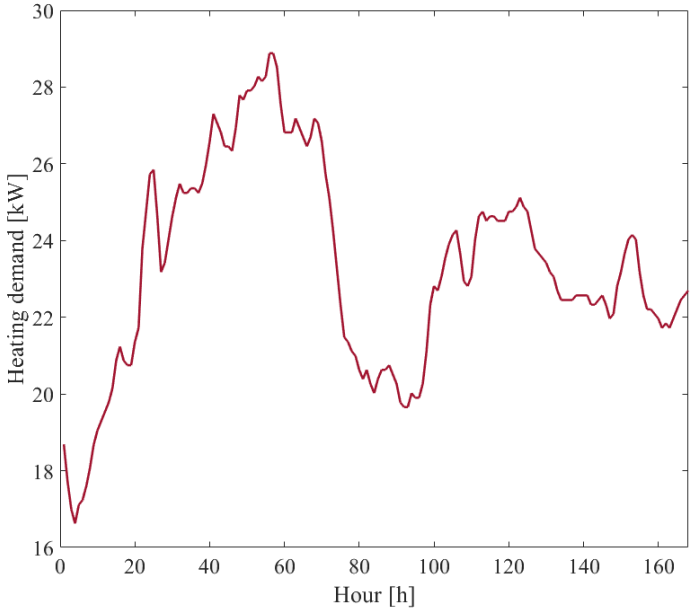

Fig. A1 A graph illustrating the hourly variations of the multi-family building's heating demand for the 1st week of January 2019.

Appendix B – IMST-ART modeling and COP_1 mapping

This appendix is intended to give the reader more details on the IMST-ART modeling used for the parametric sweep and COP_1 mapping. A variable speed compressor of model PSH051 from Danfoss was modeled according to the ANSI/AHRI Standard 540 using ARI-coefficients for the compressor power and mass flow, summarized in table B1. A total of 84 cases of different temperatures of the inlet and outlet temperatures of the secondary fluid in the condenser were simulated in IMST-ART. The conditions for the parametric sweep are summarized in table B2.

Table B1 ARI coefficients for compressor PSH051 at compressor frequency 65 Hz. Note that the values in the columns are not the actual compressor power or mass flow but instead the values of the coefficients C1, C2 etc.

	ARI coefficients	
	Compressor power [W]	Mass flow [kg/h]
C1	8326.66992	513.223207
C2	117.637001	15.6834712
C3	47.4674988	0.12877308
C4	2.07368994	0.18188892
C5	-1.9217499	0.01433783
C6	1.28141999	-0.008838
C7	0.0242656	0.00100003
C8	-0.042855	7.8585E-05
C9	0.0185455	-0.0001508
C10	0.00275667	3.5055E-05

Table B2 Summary of all the conditions for the condenser secondary fluid inlet and outlet temperature for the parametric sweep in IMST-ART.

$T_{cond,in}$	**$T_{cond,out}$**	**$T_{cond,in}$**	**$T_{cond,out}$**	**$T_{cond,in}$**	**$T_{cond,out}$**	**$T_{cond,in}$**	**$T_{cond,out}$**	**$T_{cond,in}$**	**$T_{cond,out}$**
25	65	27	65	29	65	31	65	33	65
25	60	27	60	29	60	31	60	33	61
25	55	27	55	29	55	31	55	33	57
25	50	27	50	29	50	31	50	33	53
25	45	27	45	29	45	31	45	33	49
25	40	27	40	29	40	31	40	33	45
25	35	27	35	29	35	31	35	33	41
25	30	27	30					33	37
$T_{cond,in}$	**$T_{cond,out}$**	**$T_{cond,in}$**	**$T_{cond,out}$**	**$T_{cond,in}$**	**$T_{cond,out}$**	**$T_{cond,in}$**	**$T_{cond,out}$**	**$T_{cond,in}$**	**$T_{cond,out}$**
35	65	37	65	39	65	41	65	43	65
35	61	37	62	39	62	41	62.5	43	62.5
35	57	37	59	39	59	41	60	43	60
35	53	37	56	39	56	41	57.5	43	57.5
35	49	37	53	39	53	41	55	43	55
35	45	37	50	39	50	41	52.5	43	52.5
35	41	37	47	39	47	41	50	43	50
		37	44	39	44	41	47.5	43	47.5
$T_{cond,in}$	**$T_{cond,out}$**								

45	65
45	62.5
45	60
45	57.5
45	55
45	52.5
45	50

A polynomial of the COP_1 as a function of the secondary fluid's inlet and outlet temperature was created from the results generated by the parametric sweep.The polynomial was on the form given by eq. (1), where $T_{cond,in}$ and $T_{cond,out}$ are the inlet and outlet temperatures of the secondary fluid in the condenser in degrees Celsius.

$$COP_1=A_0+B_1\cdot T_{cond,in}+B_2\cdot T_{cond,in}^2+C_1\cdot T_{cond,out}+C_2\cdot T_{cond,out}^2+D_1\cdot T_{cond,in}\cdot T_{cond,out} \quad (1)$$

The calculated values of the coefficients in the polynomial in eq. (1) are summarized in table B3 and the COP_1 mapping created with the polynomial from the parametric sweep is illustrated in Fig. B1.

Table B3 A summary of the coefficients for the polynomial curve regression for the COP_1 of the GSHP.

A_0	B_1	B_2	C_1	C_2	D_1
6.4911	-0.0206	-0.0001	-0.0772	0.0003	0.0002

In Fig.B1 a surface plot of the polynomial created from the parametric sweep is plotted with the individual data points from the parametric sweep (shown as black, filled circles).

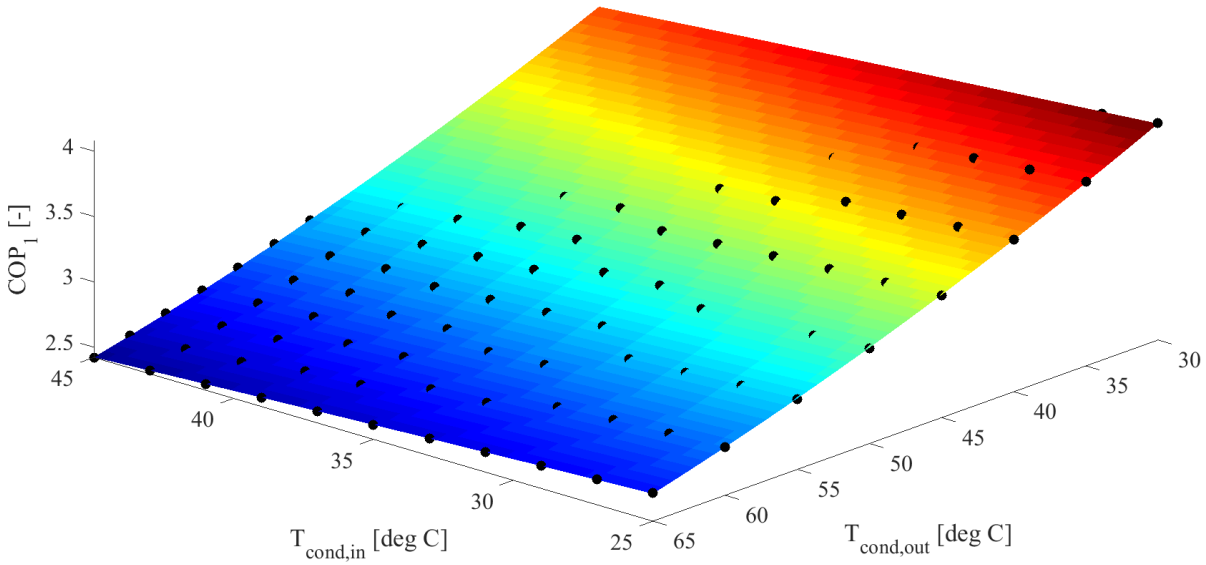

Fig. B1 The COP mapping of the GSHP model. The data points generated from the parametric sweep in IMST-ART are marked with black, filled circles and the surface is the polynomial evaluated at a fine grid of inlet and outlet temperatures of the secondary fluid of the condenser.

Appendix C - Heat loss calculation for LHTES tank

The following equation was used in the model during the LHTES's idle mode to account for heat losses to the air in the surrounding space:

$$Q_{losses}=U_L \cdot V_{tank} \cdot (T_{tank}-T_{space}) \cdot \Delta\tau \quad (1)$$

Q_{losses} – heat losses to the surrounding space [Wh]

U_L – volumetric heat loss coefficient of the tank (value established for the LHTES prototype) [W/m^3·K]

V_{tank} – total volume of the LHTES tank [m^3]

T_{tank} – temperature of the HTF in the LHTES tank [˚C]

T_{space} – temperature of the air in the surrounding space (set to 20˚C) [˚C]

$\Delta\tau$ – time period [h]

Appendix D - Bin hour analysis of peak and valley hours

Fig. D1 illustrates the histograms used for the bin hour analysis to define the peak and valley hours for the one cycle scheme used for the LHTES operation.

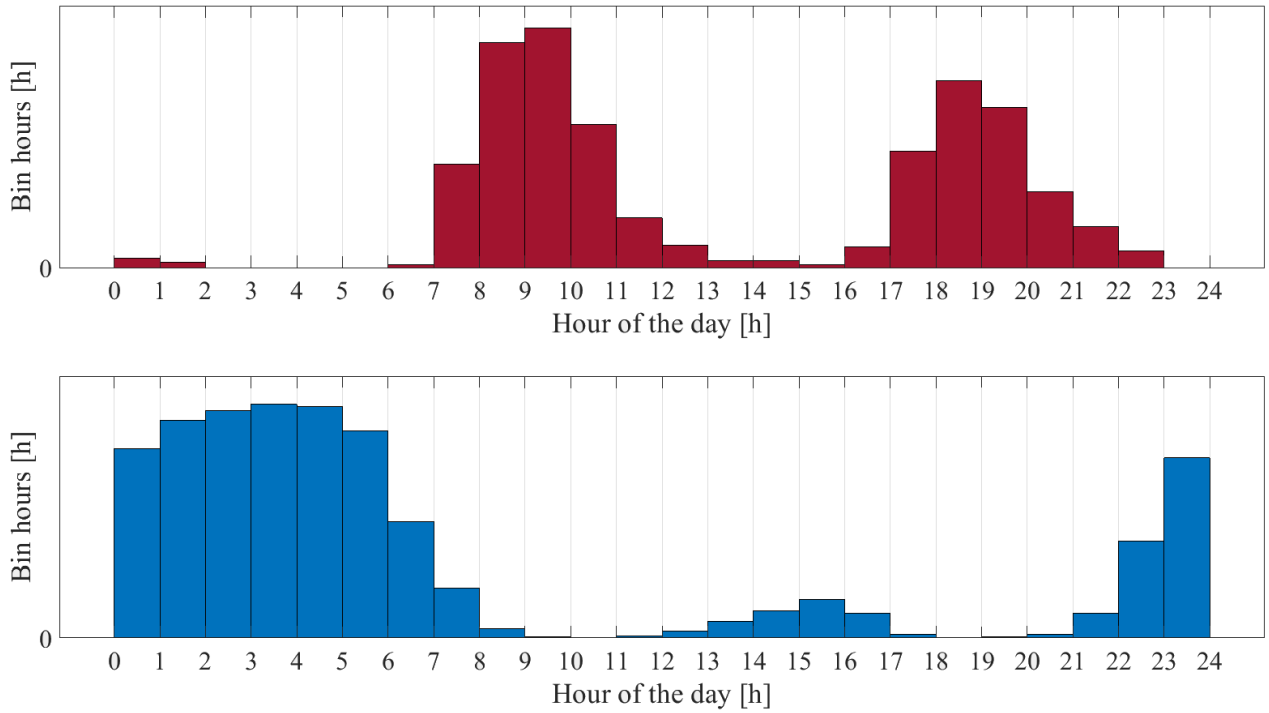

Fig. D1 Histogram over the extracted a) peak and b) valley hours.

Appendix E - Carbon dioxide emissions from power production

The hourly variations of carbon dioxide emissions related to power production are shown in fig. E1. The values shown are average values for the European Union.

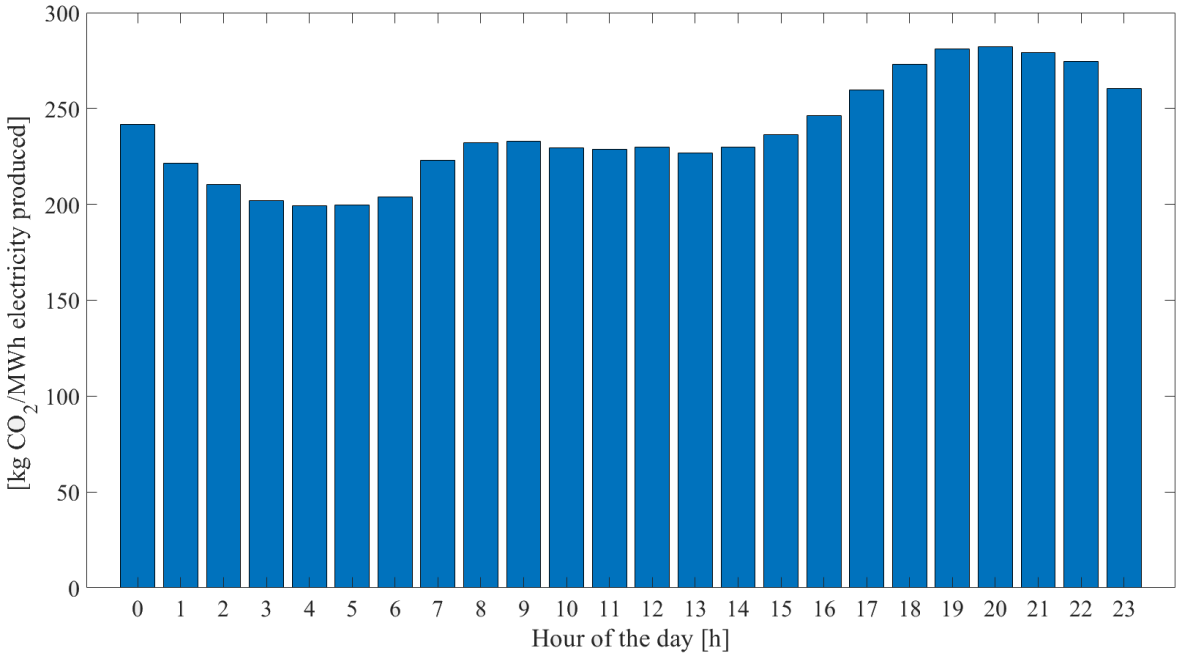

Fig. E1 Hourly variations of carbon dioxide emissions per megawatthour of produced electricity. The data presented are average values for the European Union (IEA, 2020).

TRITA TRITA-ITM-EX 2020:474